

A numerical and theoretical investigation on composite pipe-in-pipe structure under impact

Yu Wang, Xudong Qian*, J.Y. Richard Liew and Min-Hong Zhang

*Department of Civil and Environmental Engineering, Centre for Offshore Research and Engineering,
National University of Singapore, Singapore 117576*

(Received July 29, 2015, Revised October 13, 2016, Accepted November 11, 2016)

Abstract. This paper investigates the transverse impact response for ultra lightweight cement composite (ULCC) filled pipe-in-pipe structures through a parametric study using both a validated finite element procedure and a validated theoretical model. The parametric study explores the effect of the impact loading conditions (including the impact velocity and the indenter shape), the geometric properties (including the pipe length and the dimensions of the three material layers) as well as the material properties (including the material properties of the steel pipes and the filler materials) on the impact response of the pipe-in-pipe composite structures. The global impact responses predicted by the FE procedure and by the theoretical model agree with each other closely. The parametric study using the theoretical approach indicates the close relationships among the global impact responses (including the maximum impact force and the maximum global displacement) in specimens with the equivalent thicknesses, proposed in the theoretical model, for the pipe-in-pipe composite structures. In the pipe-in-pipe composite structure, the inner steel pipe, together with the outer steel pipe, imposes a strong confinement on the infilled cement composite and enhances significantly the composite action, leading to improved impact resistance, small global and local deformations.

Keywords: impact response; steel-concrete composite; dynamic analysis; sandwich composite; ultra-lightweight cement composite

1. Introduction

Concrete filled pipe-in-pipe composite structures have demonstrated enhanced structural resistance and energy absorption capacity against various external loadings in recent studies (Zhao and Han 2006, Han *et al.* 2006, Zhang *et al.* 2012) due to the steel-concrete-steel composite action. This composite structure, therefore, provides a potential solution to improve the impact resistance for onshore and offshore pipelines, threatened and damaged frequently by external interference, such as external impacts and indentations (Brooker 2005). Practical applications of such composite structures in a harsh environment require a comprehensive understanding and an extensive investigation on the transverse impact response for these pipe-in-pipe composite structures, with a large range of geometric and material properties, under various impact loading conditions.

Previous studies on the steel hollow pipes have paved a strong foundation in understanding the impact behavior of pipe-in-pipe composite structures. Researchers have carried out a large number

*Corresponding author, Associate Professor, E-mail: qianxudong@nus.edu.sg

of experimental studies on steel hollow pipes under the transverse impacts (Thomas *et al.* 1976, Jones *et al.* 1992). They further considered the internal pressure and the axial pre-load effect on the impact response for hollow pipes (Ng and Shen 2006, Jones and Birch 2010, Zeinoddini *et al.* 2002). In recent years, many researchers have utilized the finite element (FE) software, such as ABAQUS (ABAQUS 2010) and LS-DYNA (Hallquist 2006), to analyze the impact behavior of hollow pipes, as an alternative to the otherwise expensive experimental study (Zeinoddini *et al.* 2008a, b, Arabzadeh and Zeinoddini 2011, Zeinoddini *et al.* 2013, Famiyesin *et al.* 2002, Yang *et al.* 2009, Mamalis *et al.* 2010). Besides the experimental and the numerical study, researchers have also proposed some theoretical methods to estimate the dynamic response for hollow pipes under the transverse impact (Shen and Shu 2002, Wen 1997, Wen and Reid 1998). The aforementioned studies indicate that thin-walled steel hollow pipes demonstrate limited impact resistance, coupled with severe damage leading to large global deformation and local indentation. However, previous research efforts on the impact response have focused primarily on other types of composite structures (Ding *et al.* 2014, Crupi *et al.* 2011, Xie *et al.* 2014, Jankowiak *et al.* 2014, Malekzadeh 2014, Kantar and Anil 2012, Kharazan *et al.* 2014). The impact response for sandwich pipe structures remains a challenging topic due to the complexity of the dynamic problem.

This study investigates numerically and theoretically the impact response of the simply supported pipe-in-pipe composite system consisting of two steel pipes with infilled ultra-lightweight cement composite (ULCC) (Chia *et al.* 2011) in-between the two pipes (see Fig. 1). The sandwich composite pipe, also known as the double-skin composite tube, originates from the steel-concrete-steel (SCS) sandwich panels and concrete-filled pipes (CFP) in recent years (Zhao and Han 2006). Most of the research works on the sandwich composite tubular members have focused on the axial compression performance (Uenaka *et al.* 2010, Zhao *et al.* 2010, Li *et al.* 2012, Yang *et al.* 2012), the external pressure capacity (Arjomandi and Taheri 2011, An *et al.* 2012) as well as the bending behavior (Uenaka and Kitoh 2011). Wang *et al.* (2014) have recently explored experimentally the transverse impact performance of ULCC-filled pipe-in-pipe composite structures, proving the promising applications and huge potential of such composite pipes in offshore pipelines due to the significantly enhanced capacity, deformation resistance and energy absorption capability compared to steel hollow pipes. Their experimental results also demonstrate the general effect of each material layer on the impact response for the sandwich composite pipe, i.e., the outer pipe and its thickness determine directly the impact resistance and the global bending deformation; the increase in the cement composite layer thickness limits effectively the indentation of steel pipes and restricts the indentation within a high localized region around the impact location; the increase in the inner pipe thickness shows slight influence on the impact response of the pipe (Wang *et al.* 2014). However, the experimental investigation (Wang *et al.* 2014) includes a limited number of composite pipe specimens (16 specimens with only 7 geometric variations), which have the very similar material properties ($\sigma_y = 400$ MPa and $f_c = 60$ MPa) and subjected to the impact from the same drop weight releasing at a constant drop height of 3.4 m. Hence, an improved understanding on the impact response of the pipe-in-pipe composite structure requires further parametric study, which covers various impact loading conditions, geometric and material properties of the composite pipes.

This study, therefore, aims to provide a comprehensive examination on the physical responses of the pipe-in-pipe structures under lateral impacts through a parametric investigation based on the validated FE procedure (Wang *et al.* 2014) and theoretical model (Wang 2015). The FE analyses allow a detailed investigation on the geometry (for both the structure and the indenter), the material and the loading conditions of the structural system, and reveal physical responses of the

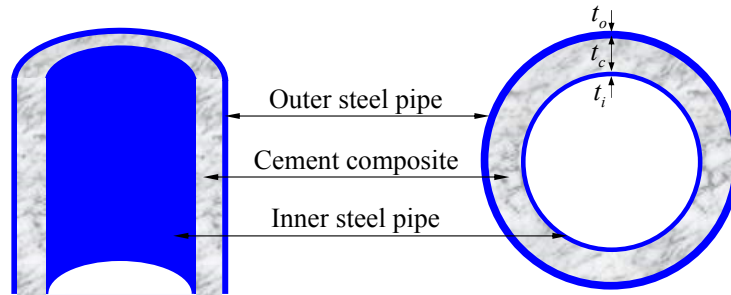


Fig. 1 The ultra-lightweight cement composite (ULCC) filled pipe-in-pipe composite structure

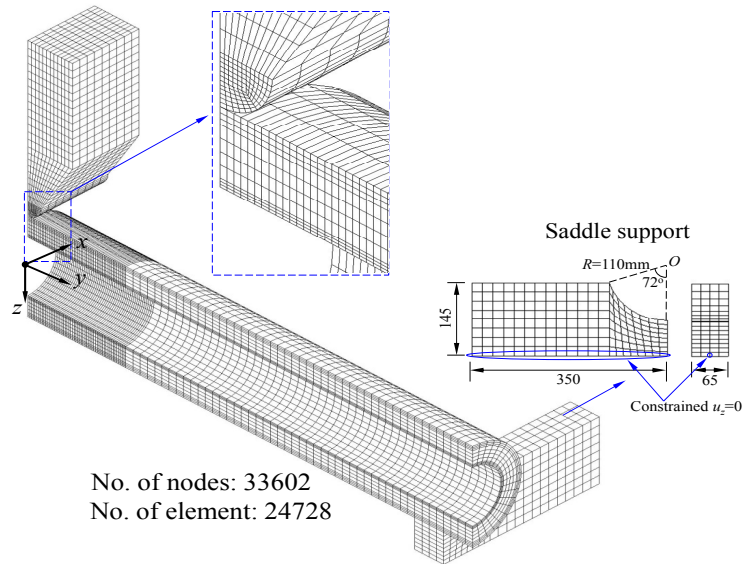
structure not previously observed during the limited-scope experimental study. The analysis by the theoretical model provides a quick examination of the global resistance of the pipe-in-pipe structure with different geometric parameters and loading conditions.

This paper starts with a brief introduction to the methodologies used in this parametric study, including the FE procedure and the theoretical method. This section also presents the scope of the parametric study. The next section investigates the effect of the impact loading condition (the impact velocity and the indenter shape), the geometric property (the pipe length and the dimensions of the three material layers) as well as the material property (the steel pipe material property and the filler material property) on the impact response of the pipe-in-pipe composite structures. The last section summarizes the conclusions drawn from this parametric study.

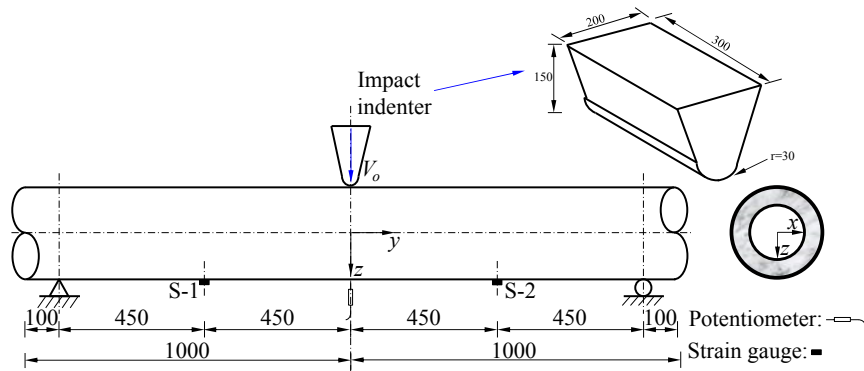
2. Methodology

2.1 Finite element procedure

The FE simulation utilizes the explicit code in the nonlinear finite element software LS-DYNA (Hallquist 2006). Fig. 2(a) shows a typical quarter-symmetric FE model for the composite pipe in the numerical analysis. All nodes on the symmetric plane remain constrained in the displacement degree of freedom perpendicular to that plane. The material property for the steel follows the J_2 plasticity model (type MAT_24 in LS-DYNA (Hallquist 2006)). The concrete damage model (type MAT_72R3 in LS-DYNA (Hallquist 2006)), developed by Malvar *et al.* (1997), is used to describe the cement composite properties. This material model employs three independent surfaces to describe the elastic-plastic behavior for the ULCC, i.e., the initial yield surface, the maximum failure surface and the residual failure surface. The steel pipes as well as the cement composite employ eight-node solid elements with reduced integration and hourglass control. Figure 2a shows a simplified saddle support model to represent the boundary conditions of the pipe specimen in the impact test. The simplified support, merged with the pipe model, rotates about a line of nodes (restrained in the vertical direction, $u_z = 0$ as highlighted in Fig. 2(a) at the bottom under the impact loading. The FE model includes the drop weight with a semi-cylindrical impact indenter ($r = 30$ mm and a width of 300 mm), as shown in Fig. 2(b) (Section 3 examines the effect of indenter shape on the impact response). After the impact test, slippage occurs between the two steel pipes and the cement composite layer. To model this incompletely bonded surface interaction, the interface between the steel pipe and the cement composite follows the automatic surface-to-surface



(a) A typical quarter-symmetric FE model for a composite pipe



(b) The simply supported pipe-in-pipe composite structure under the drop weight impact

Fig. 2 FE model and test setup for the composite pipe specimens

contact with a penalty algorithm. The interface between the impact indenter and the outer steel pipe also employs the surface-to-surface contact model. For two deformable surfaces in contact, the master surface refers usually to the stiffer body or the surface with a coarser mesh if the two surfaces have comparable stiffness (Hallquist 2006). Therefore, the FE procedure selects the steel surfaces (for both the inner and outer pipe) as the master surface as they are in contact with the cement composite (slave surface) while defines the outer steel pipe surface as the slave surface as it is in contact with the indenter (master surface). When LS-DYNA detects a penetration from the slave node into the master surface, the numerical procedure introduces a fictitious spring to simulate an interfacial force between the slave node and its corresponding node on the master surface to push the node out from the master surface.

The parametric analysis chooses one basic pipe-in-pipe specimen, CCFPIP-2-1, in the

experimental study (Wang *et al.* 2014) as the benchmark since the specimen CCFPIP-2-1 (see Table 1 and Fig. 3) represent approximately the average material and geometric properties among the total 16 composite specimens in the entire experimental program (Wang *et al.* 2014). The tensile strength of the cement composite material equals 3.4 MPa, measured from the 28-day split-cylinder tests. The numerical procedure incorporates the strain rate dependence of the cement composite and steel materials. For concrete materials under compression, the dynamic increase factor (*DIF*) on the compressive strength (in MPa) follows (CEB 1993)

$$DIF_{c,concrete} = \begin{cases} (\dot{\epsilon}_d / \dot{\epsilon}_s)^{1.026\alpha_s} & \text{for } \dot{\epsilon}_d \leq 30 \text{ s}^{-1}, \alpha_s = 1 / (5 + 9f_c / 10) \\ \gamma_s (\dot{\epsilon}_d / \dot{\epsilon}_s)^{1/3} & \text{for } \dot{\epsilon}_d > 30 \text{ s}^{-1}, \log \gamma_s = 6.156\alpha_s - 2 \end{cases} \quad (1)$$

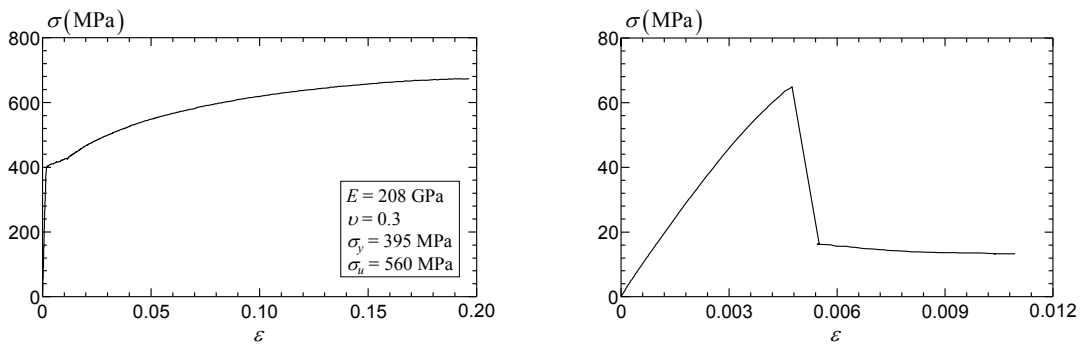
The *DIF* for the tensile strength of cement composite (in MPa) employs the recommendation by Malvar and Ross (1998)

$$DIF_{t,concrete} = \begin{cases} (\dot{\epsilon}_d / \dot{\epsilon}_s)^\delta & \text{for } \dot{\epsilon}_d \leq 1 \text{ s}^{-1}, \delta = 1 / (1 + 8f_c / 10) \\ \beta (\dot{\epsilon}_d / \dot{\epsilon}_s)^{1/3} & \text{for } \dot{\epsilon}_d > 1 \text{ s}^{-1}, \log \beta = 6\delta - 2 \end{cases} \quad (2)$$

For steel materials, the *DIF* on the yield strength adopts the commonly used Cowper and Symonds model (2008)

$$DIF_{steel} = 1 + (\dot{\epsilon}_d / C)^{1/p} = (\dot{\epsilon}_d / \dot{\epsilon}_s)^{(0.074 - 0.04\sigma_y / 414)} \quad (3)$$

Fig. 3 illustrates the uni-axial true stress-true strain relationship for the steel material and that for the cement composite material under unconfined, uniaxial compression.



(a) Uni-axial true stress-true strain relationship for steel (b) stress-strain relationship for the ULCC

Fig. 3 Material properties for CCFPIP-2-1

Table 1 Details of the benchmark specimen CCFPIP-2-1 by Wang *et al.* (2014)

Specimen	<i>L</i> (m)	<i>L_o</i> (m)	<i>D_o</i> (mm)	<i>t_o</i> (mm)	<i>D_i</i> (mm)	<i>t_i</i> (mm)	<i>t_c</i> (mm)	σ_y (MPa)	<i>f_c</i> (MPa)	ρ_c (kg/m ³)	<i>V_o</i> (m/s)	<i>m_d</i> (kg)
CCFPIP-2-1	2	1.8	219.1	6.3	139.7	5.0	33.4	395.4	64.9	1470	7.56	1350

The following discussion uses “CCFPIP-2-1” to designate sandwich composite models with the same geometric dimensions as the experimental specimen CCFPIP-2-1 in the experiment (Wang *et al.* 2014). In Table 1, m_d refers to the mass of the drop weight, which remains fixed at 1350 kg throughout this study. Fig. 4 presents the close agreement between the impact test results (Wang *et al.* 2014) and the FE analysis for CCFPIP-2-1, in both the global response of the pipe specimen (Figs. 4(a) and (b)) and the local behavior of the pipe (Figs. 4(c) and (d)). In Fig. 4, P denotes the impact force; w_g represents the global displacement, measured by the potentiometer attached to the pipe bottom at the mid-span (see Fig. 2b); δ refers to the local indentation, which equals the difference in displacement between the top surface and the bottom surface of the pipe (see Fig. 2(b)); and ε indicates the strain value measured at the quarter-span positions S-1 and S-2 (see Fig. 2(b)). The horizontal axis in Fig. 4(c) measures the distance from the center of the pipe along the longitudinal axis of the pipe (see Fig. 2). The experimental procedure measures the impact force history through three dynamic load cells connected to high-strength steel indenter, and monitors the global displacement through displacement transducers mounted on the specimen. The FE analysis computes the impact force by summing the contact force between the indenter surface and the outer surface of the pipe-in-pipe specimen.

The parametric study, using the validated FE procedure, investigates the effect of the impact velocity ($V_o \in [2.5 \text{ m/s}, 10.0 \text{ m/s}]$), the indenter shape (semi-cylindrical indenter with $r \in [15 \text{ mm}, 60 \text{ mm}]$ and flat head indenter with a width of 60 mm), the pipe length ($L \in [2 \text{ m}, 6 \text{ m}]$), the steel

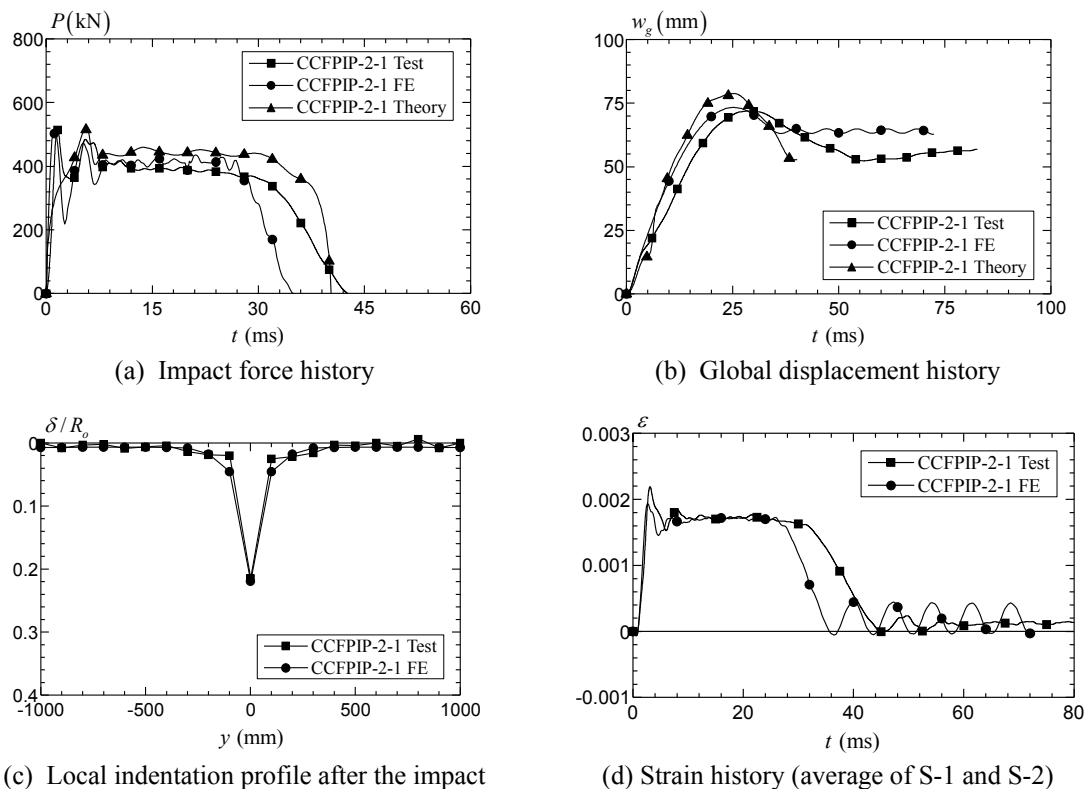


Fig. 4 Comparison of the impact response between the test data, the FE results and the theoretical predictions for CCFPIP-2-1 by Wang *et al.* (2014)

pipe strength ($\sigma_y \in [250 \text{ MPa}, 690 \text{ MPa}]$) as well as the filler material strength ($f_c \in [30 \text{ MPa}, 110 \text{ MPa}]$) on the impact response of pipe-in-pipe composite structures. In addition, the parametric study explores the inner pipe effect on the impact behavior for the sandwich composite pipe by comparing the response of two pipe-in-pipe composite models with different inner pipe thicknesses ($t_i = 50 \text{ mm}$ and 6.3 mm respectively), one composite pipe model without inner pipe and one steel hollow pipe model in the FE analyses. Furthermore, the parametric study examines the impact response for pipe-in-pipe composite models with different filler materials, including the ULCC, the normal weight concrete and the high strength grout, by applying specific coefficients respectively in the material model (type MAT_72R3 in LS-DYNA (Hallquist 2006)) based on the material test data.

2.2 Theoretical model

Wang (2015) has proposed a theoretical model to estimate the global response for pipe-in-pipe composite structures under the transverse impact, including the impact force response and the global displacement response. The theoretical model integrates a validated load-indentation ($P-\delta$) relationship, derived by an analytical two-stage approach (Qian *et al.* 2015), into the deformation response of the sandwich composite pipe

$$\delta = w_i - w_g \tag{4}$$

where w_i denotes the total deflection at the impact location on the pipe and w_g refers to the global displacement of the pipe.

The theoretical model assumes that the displacement for the impact indenter equals the total deflection at the impact location on the pipe, i.e., the impact indenter remains in contact with the pipe throughout the impact process. The displacement for the indenter (also the total deflection at the impact location on the pipe w_i) at time t follows (Lee 1940)

$$w_i(t) = V_o t - \frac{1}{m_d} \int_0^t P(\tau)(t - \tau) d\tau \tag{5}$$

where V_o refers to the initial impact velocity and m_d denotes the mass of the drop weight, i.e., 1350 kg in this study. P represents the transverse impact force, varying with the time.

The global displacement (w_g) for the pipe consists of two parts

$$w_g = w_{g,e} + w_{g,p} \tag{6}$$

where $w_{g,e}$ and $w_{g,p}$ refer to the elastic and the plastic global displacement of the pipe, respectively. The theoretical method treats the simply supported pipe as a beam and employs Timoshenko's beam theory (Lee 1940, Goldsmith 1960) to calculate the elastic displacement. At time t , the elastic global displacement at the mid-span of the pipe follows (Lee 1940, Goldsmith 1960)

$$w_{g,e}(t) = \frac{2}{m_p} \sum_{i=1,3,\dots}^{\infty} \frac{1}{\omega_i} \int_0^t P(\tau) \sin[\omega_i(t - \tau)] d\tau \tag{7}$$

in which m_p refers to the total mass of the pipe and ω_i defines the i^{th} angular frequency of the

natural vibration for the pipe ($i = 1, 3, 5 \dots$).

The theoretical model derives the plastic global displacement ($w_{g,p}$) through an energy approach, which assumes that the plastic hinge at the mid-span dissipates all the global plastic energy ($E_{g,p}$) for the simply supported pipe and ignores energy losses during the impact

$$E_{g,p} = 2M_p \theta = \frac{4M_p}{L_o} w_{g,p} \quad (8)$$

$$w_{g,p} = \frac{E_{g,p} L_o}{4M_p} = \frac{(E_d - E_\delta - E_{g,e}) L_o}{4M_p} \quad (9)$$

where M_p denotes the plastic moment capacity of the pipe cross section at the mid-span. θ and L_o represent the rotation at the support and the clear span length of the pipe, respectively. E_d , E_δ and $E_{g,e}$ refer to the kinematic energy, the local indentation energy and the elastic global deformation energy for the pipe, respectively.

On the other hand, the two-stage approach (Qian *et al.* 2015) estimates the P - δ relationship for pipe-in-pipe composite structures in two different phases, i.e., the composite stage and the separation stage. In the composite stage, the analytical approach extends a theoretical shell model (see Fig. 5) for steel hollow pipe (Wierzbicki and Suh 1988), consisting of a ring model (see Fig. 5(b)) and a generator model (see Fig. 5(c)), to the current sandwich pipes. The bending in the ring model and the extension in the generator model contribute to the load capacity of the pipe structure. In the ring model, the plastic moment capacity of the steel hollow pipe wall with a unit width follows

$$M_o = \frac{1}{4} \sigma_y t_o^2 \quad (10)$$

For sandwich composite pipes, the equivalent plastic moment capacity, M_o , of the sandwich pipe wall with a unit width depends on the location of the neutral axis, and follows the below expressions for four different situations. For $t_o > t_i$ and $f_c < \sigma_y(t_o - t_i)/t_c$

$$M_o = \frac{\sigma_y}{4} \left[(t_o + t_i)^2 + 4t_c t_i + \frac{2f_c t_c (t_o + t_c - t_i)}{\sigma_y} - \frac{f_c^2 t_c^2}{\sigma_y^2} \right] \quad (11)$$

For $t_o > t_i$ and $f_c > \sigma_y(t_o - t_i)/t_c$

$$M_o = \frac{\sigma_y}{4} \left[\frac{4f_c t_o t_c + 2f_c(t_o^2 + t_i^2) - 2\sigma_y(t_o - t_i)^2}{f_c} \right] \quad (12)$$

For $t_o = t_i$

$$M_o = \sigma_y t_o (t_c + t_o) \quad (13)$$

For $t_o < t_i$

$$M_o = \frac{\sigma_y}{4} [(t_o + t_i)^2 + 4t_o t_c] \quad (14)$$

The above calculation of M_o ignores the tensile strength of the cement composite. Therefore, the equivalent thickness in the sandwich composite pipe for the ring model t_{ring} , becomes, for $t_o > t_i$ and $f_c < \sigma_y(t_o - t_i)/t_c$

$$t_{ring} = \sqrt{(t_o + t_i)^2 + 4t_c t_i + \frac{2f_c t_c (t_o + t_c - t_i)}{\sigma_y} - \frac{f_c^2 t_c^2}{\sigma_y^2}} \quad (15)$$

For $t_o > t_i$ and $f_c > \sigma_y(t_o - t_i)/t_c$

$$t_{ring} = \sqrt{\frac{4f_c t_o t_c + 2f_c(t_o^2 + t_i^2) - 2\sigma_y(t_o - t_i)^2}{f_c}} \quad (16)$$

For $t_o = t_i$

$$t_{ring} = 2\sqrt{t_o(t_c + t_o)} \quad (17)$$

For $t_o < t_i$

$$t_{ring} = \sqrt{(t_o + t_i)^2 + 4t_o t_c} \quad (18)$$

In the generator model, the axial capacity of the steel hollow pipe wall with a unit width follows

$$N_o = \sigma_y t_o \quad (19)$$

Neglecting the cement composite in tension, the equivalent axial capacity, N_o , of the sandwich

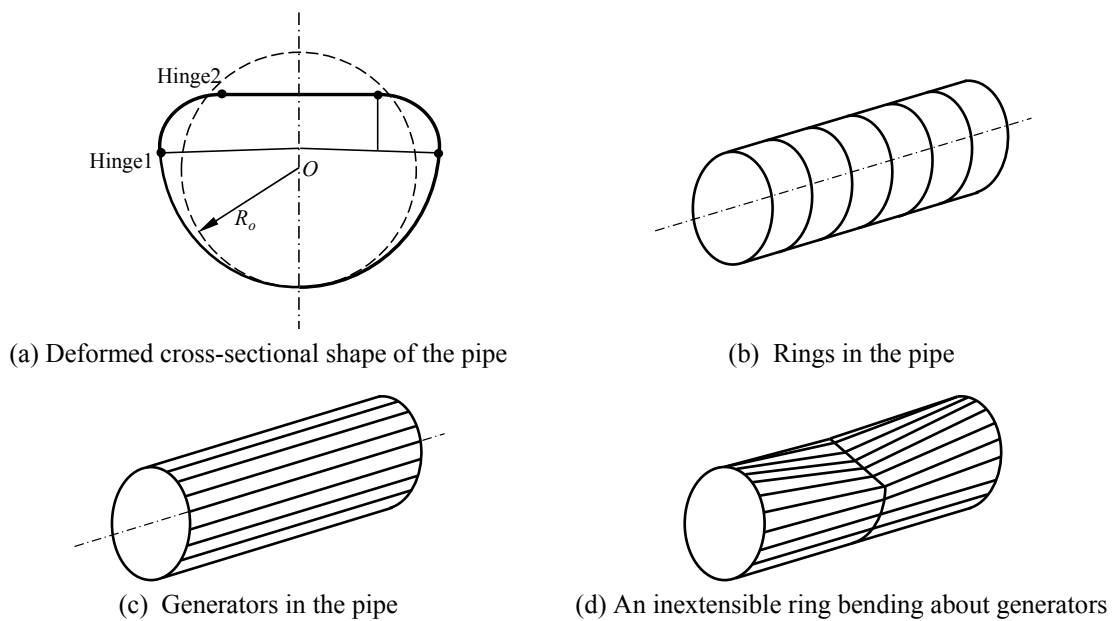


Fig. 5 A simplified shell model

composite pipe wall with a unit width becomes

$$N_o = \sigma_y(t_o + t_i) \quad (20)$$

Hence, the equivalent thickness in the sandwich composite pipe for the generator model, t_{gen} , follows

$$t_{gen} = t_o + t_i \quad (21)$$

Using a similar approach for steel hollow pipes by Wierzbicki and Suh (1988), the P - δ relationship for the current sandwich pipes in the first composite stage becomes

$$P = \sigma_y t_{ring} \sqrt{2\pi t_{gen} \delta} \quad (22)$$

With the increasing local indentation, the large deformation in the steel pipe and the cement composite failure leads to the separation of the originally in contact steel and cement composite surfaces. The loss of contact between the two materials dismisses the composite action and causes a slower increase in the pipe resistance as the indentation increases. Thus, the P - δ relationship of the sandwich pipe enters into the second stage, namely the separation stage. In this phase, the indentation resistance derives from three individual layers of materials (Qian *et al.* 2015)

$$P = P_o + P_i + P_c \quad (23)$$

in which P_o , P_i and P_c represent the indentation resistance contributed by the outer pipe, the inner pipe and the cement composite layer respectively.

Substituting Eqs. (5), (6), (7), (9) and the two-stage P - δ relationship (Eqs. (22) and (23)) into the deformation response of the sandwich composite pipe under the transverse impact (Eq. (4)), leads to an equilibrium function with an unknown impact force history. Using a numerical procedure (Wang *et al.* 2015), the theoretical method solves iteratively the equilibrium function to determine the global impact response for the pipe-in-pipe composite structures, including the impact force history and the global displacement history.

Fig. 4 demonstrates the reasonable agreement between the test data (Wang *et al.* 2014) and the theoretical predictions for the global impact response of CCFPIP-2-1, including the impact force history (Fig. 4(a)) and the global displacement history (Fig. 4(b)). The theoretical method provides a quick and reasonable prediction on the global impact response (including the global impact resistance and the maximum global displacement) for pipe-in-pipe composite structures, as an alternative to the computationally demanding FE analysis and the expensive experimental approach.

Compared to the FE procedure, the theoretical model treats the composite pipe as a beam, leading to the difficulty in providing accurate local details of the impact response, including the indentation profile, the strain values, etc. In the above theoretical model, the two-stage P - δ relationship (Eqs. (22) and (23)) ignores the indenter shape differences in the first composite stage [see Eq. (22)]. Nevertheless, this paper employs the theoretical method to investigate the effect of the impact velocity ($V_o \in [2.5 \text{ m/s}, 10.0 \text{ m/s}]$), the pipe length ($L \in [2 \text{ m}, 6 \text{ m}]$), the steel pipe strength ($\sigma_y \in [250 \text{ MPa}, 690 \text{ MPa}]$) as well as the cement composite strength ($f_c \in [30 \text{ MPa}, 110 \text{ MPa}]$) on the global response of the pipe-in-pipe composite structures. The parametric study based on the theoretical method covers a wide range of geometric properties for the pipe-in-pipe

composite structures ($D_o/t_o \in [21.9, 43.8]$, $D_i/t_i \in [11.4, 42.1]$ and $t_c \in [15.4 \text{ mm}, 44.4 \text{ mm}]$) subjected to various impact velocities ($V_o \in [2.5 \text{ m/s}, 10.0 \text{ m/s}]$).

3. Results and discussion

3.1 Effect of the impact loading condition

This section investigates the impact response for pipe-in-pipe composite structures under various impact loading conditions, including different impact velocities and impact using different indenters. Table 2 and Fig. 6 present the impact response for CCFPIP-2-1 under various impact velocities, predicted by the FE analysis and the theoretical model. In Table 2, “V1”, “V2”, “V3” and “V4” denote the initial impact velocity (V_o) of 10.0 m/s, 7.5 m/s, 5.0 m/s and 2.5 m/s, respectively. These four initial impact velocities belong to the low impact velocity, i.e., $V_o \leq 10 \text{ m/s}$ as defined in (Richardson and Wishear 1996), since most of the external impacts for offshore pipelines are low-velocity impacts (DNV-RP-F107 2010, DNV-RP-F111 2010). The low-velocity impact causes negligible strain-rate dependence of the steel and cement composite materials in the pipe-in-pip composite structures, as confirmed by Wang *et al.* (2014). The four FE analyses employ the same steel and cement composite strength, i.e., $\sigma_y = 400 \text{ MPa}$ and $f_c = 60 \text{ MPa}$, with the stress-strain relationship illustrated in Fig. 3. The force P_m (see Table 2) refers to the post-peak mean force, proposed in (Wang *et al.* 2014), to estimate the impact force in the stable phase

$$P_m = \frac{\int_{w_o}^{w_{max}} P dw_g}{w_{max} - w_o} \tag{24}$$

where w_o denotes the global displacement when the impact force (P) reaches its maximum value P_{max} and w_{max} defines the maximum global displacement. The force P_m represents an equivalent force that produces the same amount of post-peak work as the dynamic impact force and provides a good reference to the real structural resistance under the transverse impact (Wang *et al.* 2014). In general, the global impact responses predicted by the FE procedure agrees closely with that estimated by the theoretical model, as shown in Table 2. Compared to the FE analysis, the theoretical method overestimates slightly the post-peak mean force (P_m) since the theoretical method ignores the cement composite failure during the impact, as discussed in Section 2.2.

Table 2 Impact response for CCFPIP-2-1 under various impact velocities from FE analyses and theoretical predictions

Case	V_o (m/s)	E_i (kJ)	P_{max} (kN)			w_{max} (mm)			P_m (kN)			δ_{max} (mm)
			FE	Theory	Theory/FE	FE	Theory	Theory/FE	FE	Theory	Theory/FE	
V1	10.0	67.5	647.3	588.9	0.91	127.8	139.5	1.09	408.6	457.0	1.12	36.3
V2	7.5	38.0	508.2	521.7	1.03	73.5	77.2	1.05	402.7	447.8	1.11	23.9
V3	5.0	16.9	459.3	461.0	1.00	34.8	34.7	1.00	388.9	407.8	1.05	17.9
V4	2.5	4.2	362.6	383.8	1.06	10.5	9.1	0.87	323.8	332.6	1.03	8.4

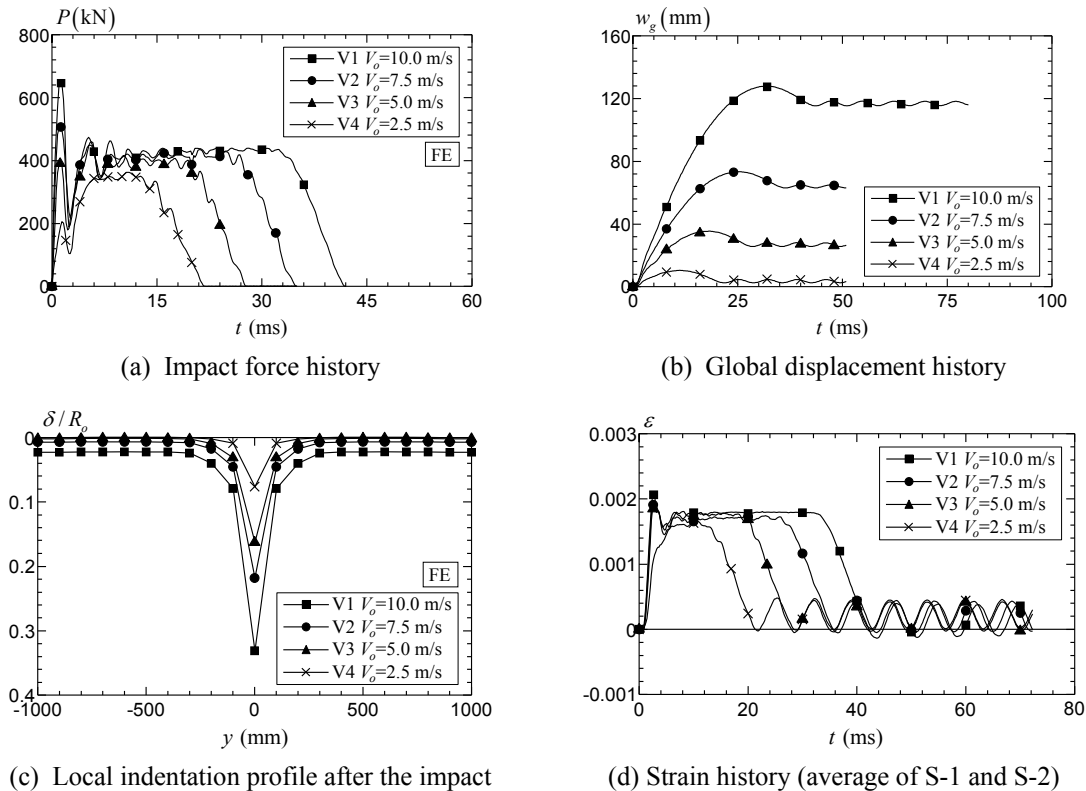


Fig. 6 Comparison of the impact response (predicted by the FE procedure) for CCFPIP-2-1 under different impact velocities

The impact force history consists generally of three phases, i.e., the vibration phase, the stable phase and the unloading phase, as illustrated in Fig. 6(a). However, the composite pipe in the case *V*4 (under a low impact velocity, 2.5 m/s) exhibits a very short stable phase with a relatively low impact resistance, caused by the low impact energy. At the very beginning of the impact, the composite pipe requires a high impact force to accelerate from a zero velocity to a speed approaching that of the drop weight. Therefore, the increase in the impact velocity, i.e., the initial velocity of the drop weight, leads to the significant rise in the maximum impact force (P_{\max}), as shown in Fig. 6(a). The increase in the impact velocity (from 5.0 m/s to 10.0 m/s), however, demonstrates small influences on the post-peak mean force (P_m) since P_m provides a good reference to the real structural resistance of the pipe-in-pipe composite member under the transverse impact. The force P_m for case *V*4 is smaller (about 20%) than that for the other three cases as the relatively low impact energy is insufficient to mobilize the full impact resistance of the pipe. Figs. 6(b) and (c) compare the global displacement histories and the local indentation profiles, respectively, for CCFPIP-2-1 under various impact velocities. The increase in the impact velocity implies the increment of the impact energy and thus intensifies both the global and the local deformations. Figure 6d indicates the marginal increase in the strain values at the positions S-1 and S-2 (at the quarter-span of the pipe) with the increase of the impact velocity since the cement composite restrains effectively the large deformation in the outer steel pipe at the quarter-span position.

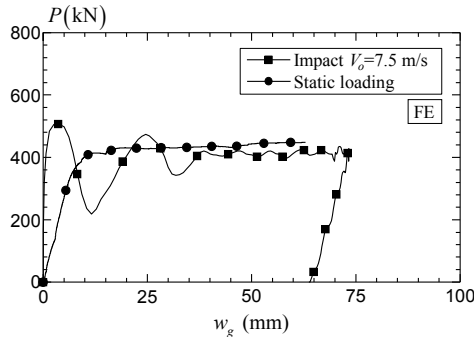


Fig. 7 Comparison of the transverse force versus the global displacement curve for CCFPIP-2-1 under the impact load ($V_o = 7.5$ m/s) and the static load

This study also investigates the behavior of the pipe-in-pipe composite specimen under the static load at the mid-span. The static FE analysis uses the same FE model, including the boundary conditions, the geometric and the material properties, as the dynamic model, but employs the implicit solver in LS-DYNA (Hallquist 2006). Fig. 7 compares the force versus the global displacement ($P-w_g$) curve for CCFPIP-2-1 under an impact load of $V_o = 7.5$ m/s and that subjected to a static load. Unlike the dynamic $P-w_g$ curve with three phases, the static $P-w_g$ curve shows a slow increase to a plateau and maintains this plateau to a large deformation level ($w_g/R = 0.6$). The load resistance (i.e., the force corresponding to the plateau) in the static FE analysis shows a magnitude close to the post-peak mean force (P_m) in the dynamic FE analysis since both of them represent the structural strength for CCFPIP-2-1.

The impact test program by Wang *et al.* (2014) employs a drop weight with a semi-cylindrical impact indenter ($r = 30$ mm), as shown in Fig. 2(b). This parametric study compares the impact response (predicted by the FE procedure) for CCFPIP-2-1 under the impact using indenters with different shapes and sizes, as presented in Table 3 and Fig. 8. In Table 3, “r1”, “r2” and “r3” denote the FE simulations using a semi-cylindrical indenter with the radius of 60 mm, 30 mm and 15 mm, respectively, while the “Flat head” refers to the FE simulation containing a flat-head indenter with a half width (in the y direction in Fig. 2) of 30 mm. The indenter length (in the x direction in Fig. 2) for the four simulation cases remains fixed at 300 mm. The four simulation cases utilize the same steel and cement composite strength, i.e., $\sigma_y = 400$ MPa and $f_c = 60$ MPa, as well as the same initial impact velocity ($V_o = 7.5$ m/s).

The initial phase of the impact engages an apparently larger contact area between the pipe and the flat-head indenter than that between the pipe and the semi-cylindrical indenter, leading to the highest maximum impact force (P_{max}) for the flat head indenter, as shown in Fig. 8(a). The

Table 3 Impact response for CCFPIP-2-1 subjected to the impact from different indenters from FE analyses

Case	r (mm)	P_{max} (kN)	w_{max} (mm)	P_m (kN)	δ_{max} (mm)
r1	60	538.9	74.0	405.5	22.7
r2	30	508.2	73.5	402.7	23.9
r3	15	506.3	72.8	394.7	24.7
Flat head	-	627.9	75.0	396.5	19.7

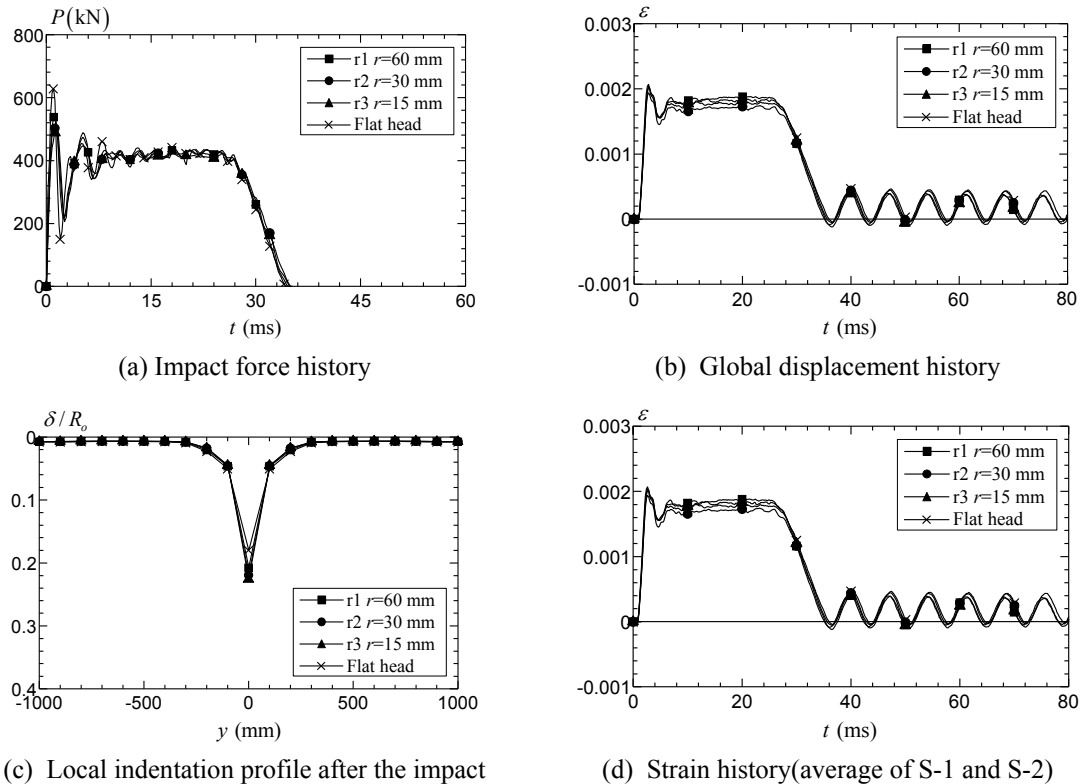


Fig. 8 Comparison of the impact response (predicted by the FE procedure) for CCFPIP-2-1 under different impact velocities

maximum impact forces (P_{\max}) for the other three simulation cases (from $r1$ to $r3$) maintain a similar magnitude due to the marginal differences in the contact area among the three cases. The increase in the radius of the semi-cylindrical indenter, however, does lead to slight increases in the maximum impact force (P_{\max}) and the post-peak mean force (P_m), as listed in Table 3. Figure 8b illustrates the similar global displacement response for the composite pipe subjected to the impact using different indenters with the same external impact energy ($E_i = 38.0$ kJ). The increase in the contact area causes marginal deviations (within 3%) in the maximum global displacement for the composite pipe, as presented in Table 3. The increase in the contact area during the impact expands the indentation zone, leading to an enhanced resistance against the local indentation and a decrease in the indentation depth. Hence, the composite pipe under the flat-head indenter impact experiences the smallest local indentation, followed by the pipe under a semi-cylindrical indenter with the radius equal to 60 mm ($r1$), 30 mm ($r2$) and 15 mm ($r3$), as shown in Table 3 and Fig. 8(c). Fig. 8(d) elucidates the close responses in the strain history at the positions S-1 and S-2 in the four FE simulation cases.

3.2 Effect of the geometric properties

The previous experimental study included only 16 pipe-in-pipe composite specimens with the same pipe length ($L = 2$ m) and very limited dimension variations in the outer pipe, the inner pipe

and the cement composite layer (Wang *et al.* 2014). This parametric study covers a large range of geometric properties, including the pipe length ($L \in [2 \text{ m}, 6 \text{ m}]$) and the dimensions of the three material layers ($D_o/t_o \in [21.9, 43.8]$, $D_i/t_i \in [11.4, 42.1]$ and $t_c \in [15.4 \text{ mm}, 44.4 \text{ mm}]$), for the pipe-in-pipe composite structures under the transverse impact. In addition, this study compares the impact response for different kinds of pipe structures to examine the effect of the inner steel pipe in providing confinement to the cement composite.

Table 4 Impact response for pipe-in-pipe composite model with different length from FE analyses and theoretical predictions

Case	L (m)	L_o (m)	P_{\max} (kN)			w_{\max} (mm)			P_m (kN)			δ_{\max} (mm)
			FE	Theory	Theory/FE	FE	Theory	Theory/FE	FE	Theory	Theory/FE	FE
L1	2	1.8	508.2	521.7	1.03	73.5	77.2	1.05	402.7	447.8	1.11	23.9
L2	3	2.8	578.3	419.7	0.73	128.2	138.5	1.08	270.4	260.2	0.96	18.4
L3	4	3.8	542.9	283.5	0.52	186.4	187.8	1.01	195.4	194.8	1.00	15.5
L4	6	5.8	548.8	221.9	0.40	340.9	311.4	0.91	120.2	122.8	1.02	13.5

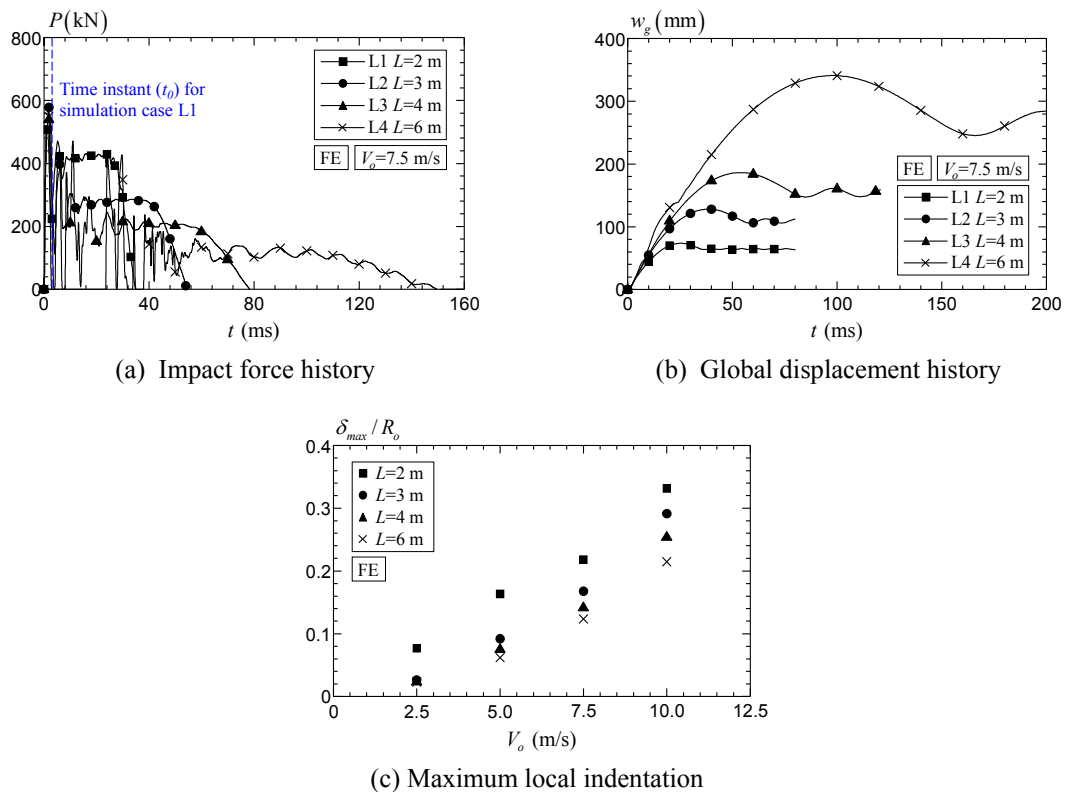


Fig. 9 Comparison of the impact response (predicted by the FE procedure) for pipe-in-pipe composite models with different length

Table 4 demonstrates the impact response for pipe-in-pipe composite models with the same dimensions as CCFPIP-2-1 but different pipe lengths. In Table 4, “L1”, “L2”, “L3” and “L4” denote the simulation case with the pipe length of 2 m, 3 m, 4 m and 6 m respectively. The four cases utilize the same steel and cement composite strength, i.e., $\sigma_y = 400$ MPa and $f_c = 60$ MPa (see Fig. 3), as well as the same initial impact velocity ($V_o = 7.5$ m/s). Figures 9 and 10 present the impact response for the pipe-in-pipe composite structures predicted by the FE procedure and the theoretical method.

With the increase of the pipe length, the flexibility of the pipe increases significantly. In the FE simulations for cases L2, L3 and L4, the top surface of the pipe at the impact location experience a larger downward displacement than that of the indenter after the first strike, leading to the separation between the pipe and the indenter and thus a zero impact force (see Fig. 9(a)). The impact force regains quickly once the pipe and the indenter contact with each other again. The pipe specimen may experience multiple separations from the indenter and vibrate severely during the initial phase of the impact, as exemplified by the 6 m long pipe (case L4) in Fig. 9(a). Due to the increased flexibility with the increasing pipe length, the longer pipe specimens sustain a lower impact load, as a significant portion of the impact energy dissipates through the vibration of the pipes, as indicated by the P_{\max} and P_m values in Table 4. For similar reasons, the global displacement of the pipe at the mid-span increases with the increase in the pipe length, as shown in Fig. 9(b). Figs. 9(c) illustrates the maximum local indentation (δ_{\max}) for pipe-in-pipe composite models (outer pipe 219.1×6.3 and inner pipe 139.7×5) with four different pipe lengths, i.e., $L = 2$ m, 3 m, 4 m and 6 m, subjected to four various impact velocities, i.e., $V_o = 2.5$ m/s, 5 m/s, 7.5 m/s and 10 m/s. Under the same impact velocity, the increase in the pipe length leads to the decrease in the maximum local indentation (δ_{\max}) since long pipes are more flexible to bend globally and thus dissipate more impact energy by the global deformation. Consequently, this leads to a lower impact energy absorbed by the local indentation compared to short pipes. The increase in the impact velocity intensifies the maximum local indentation (δ_{\max}) due to the increment of the external impact energy.

To further investigate the zero impact force phenomenon for long pipes in the FE analyses, this study introduces a parameter named as momentum ratio (R_m)

$$R_m = \frac{\int_0^{t_0} P dt}{m_d V_o} \quad (25)$$

where m_d refers to the mass of the drop weight and V_o represents the initial impact velocity. t_0 denotes the time instant when the impact force (P) decreases to zero or to the bottom of the force valley after the initial strike. In the current FE simulations, the impact force becomes zero at the time instant t_0 for cases L2, L3 and L4 while reduces to a non-zero value at the bottom of a force valley for case L1, as illustrated in Fig. 9(a). Table 5 summarizes the momentum ratio for both pipe-in-pipe composite models (outer pipe 219.1×6.3 and inner pipe 139.7×5) and hollow pipe models (219.1×10) with four different pipe lengths, i.e., $L = 2$ m, 3 m, 4 m and 6 m, under four various impact velocities, i.e., $V_o = 2.5$ m/s, 5 m/s, 7.5 m/s and 10 m/s respectively, in the FE analyses. In Table 5, the momentum ratio in bold indicates the separation of the pipe specimen from the indenter. The momentum ratio (R_m) reflects the amount of the momentum transferred from the drop weight to the pipe during the first strike. With the increase of the pipe length and the decrease of the impact velocity, the momentum ratio increases gradually, as presented in Table 5.

Table 5 Momentum ratio (R_m) for pipe-in-pipe models and hollow pipe models in FE analyses

	L (m)	V_o (m/s)			
		2.5	5.0	7.5	10.0
Pipe-in-pipe (219.1×6.3 & 139.7×5.0)	2	0.105	0.094	0.095	0.083
	3	0.119	0.111	0.102	0.098
	4	0.154	0.148	0.139	0.131
	6	0.243	0.237	0.225	0.209
Hollow pipe (219.1×10.0)	2	0.056	0.044	0.035	0.030
	3	0.108	0.095	0.094	0.079
	4	0.122	0.106	0.101	0.095
	6	0.176	0.161	0.147	0.136

The higher the momentum ratio implies that the pipe specimen undergoes a larger velocity, which facilitates the separation between the pipe and the indenter, i.e., the zero impact force phenomenon.

Compared to the FE data, the theoretical method underestimates significantly the maximum impact force (P_{max}) for the sandwich composite pipe in cases $L2$, $L3$ and $L4$, with the length of 3 m, 4 m and 6 m respectively, as listed in Table 4. The theoretical method assumes the impact indenter remains in contact with the pipe throughout the impact process (Wang 2015), forcing a misrepresentation of the contact phenomenon in the initial strikes. However, the theoretical approach provides accurate predictions on the maximum global displacement (w_{max}) and the post-peak mean force (P_m) for these long composite pipes, as shown in Table 4. These maximum global displacements and the post-peak mean forces represent the response of the pipe specimen under the impact loading in an average sense. Since the total impact energy and the total momentum created by the impact remains independent of the separation phenomenon, the theoretical model still provides reasonable estimates on these quantities compared to the FE results.

Fig. 10(c) demonstrates the post-peak mean force (P_m), predicted by both the FE procedure and the theoretical model, for pipe-in-pipe composite models (outer pipe 219.1×6.3 and inner pipe 139.7×5) with four different pipe length, i.e., $L = 2$ m, 3 m, 4 m and 6 m, subjected to four various impact velocities, i.e., $V_o = 2.5$ m/s, 5 m/s, 7.5 m/s and 10 m/s. The post-peak mean force (P_m) decreases with the increase in the pipe length due to the increasing bending flexibility for long pipes. The increase in the impact velocity imposes slight influences on the post-peak mean force (P_m) especially for relatively higher impact velocities $V_o = 5$ m/s, 7.5 m/s and 10 m/s (see Fig. 10(c)). This indicates that the impact with $V_o \geq 5$ m/s has sufficient energy to mobilize the full impact resistance in the composite pipes. This also reflects that the post-peak mean force (P_m) provides a good reference to the real structural strength under the transverse impact regardless of the external impact loading conditions.

The parametric study further investigates the impact response for fifteen pipe-in-pipe composite members under four different impact velocities ($V_o = 10$ m/s, 7.5 m/s, 5.0 m/s and 2.5 m/s) by the theoretical method. The fifteen sandwich composite pipes have fixed length of 2 m and cover three types of relationships between the outer pipe thickness and the inner pipe thickness, i.e., $t_o > t_i$ [including the two conditions for t_{ring} as defined in Eqs. (15) and (16) respectively], $t_o = t_i$ and $t_o < t_i$, as well as a wide range of the geometric properties ($D_o/t_o \in [21.9, 43.8]$, $D_i/t_i \in [11.4, 42.1]$ and $t_c \in [15.4 \text{ mm}, 44.4 \text{ mm}]$), as listed in Table 6. Table 6 also presents the equivalent

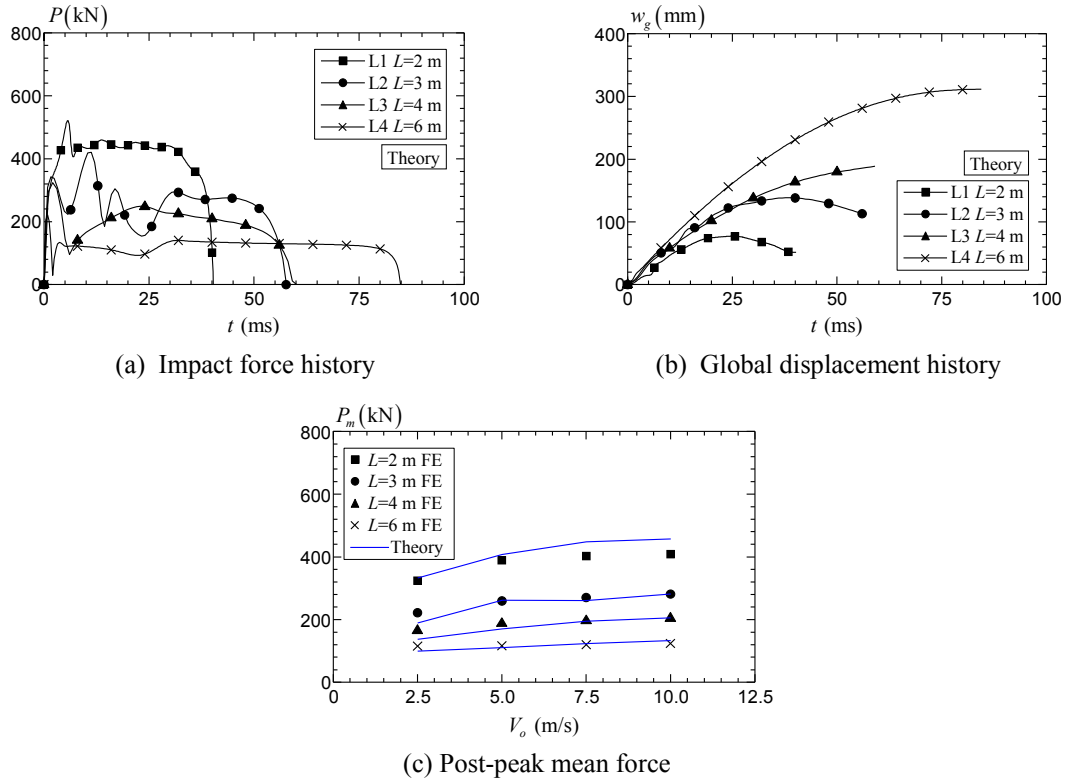


Fig. 10 Comparison of the impact response for pipe-in-pipe composite models with different length

Table 6 Dimensions for pipe-in-pipe composite members in the theoretical parametric study

	Eq. for t_{ring}	D_o (mm)	t_o (mm)	D_i (mm)	t_i (mm)	t_c (mm)	t_{ring} (mm)	t_{gen} (mm)	$\frac{D_o}{t_{gen}}$	$\frac{D_o}{t_{gen}}$	$\frac{D_o}{\sqrt{t_{gen}t_{ring}}}$
$t_o > t_i$	Eq. (15)	219.1	10	168.3	4	15.4	23.2	14.0	15.7	9.4	12.2
		219.1	10	139.7	5	29.7	33.3	15.0	14.6	6.6	9.8
	Eq. (16)	219.1	6.3	168.3	4	19.1	22.9	10.3	21.3	9.6	14.3
		219.1	5	168.3	4	20.4	21.8	9.0	24.3	10.0	15.6
		219.1	10	139.7	6.3	29.7	35.8	16.3	13.4	6.1	9.1
		219.1	6.3	139.7	5	33.4	30.8	11.3	19.4	7.1	11.7
		219.1	5	139.7	4	34.7	27.6	9.0	24.3	7.9	13.9
$t_o = t_i$	Eq. (17)	219.1	8	114.3	4	44.4	37.0	12.0	18.3	5.9	10.4
		219.1	6.3	168.3	6.3	19.1	25.3	12.6	17.4	8.7	12.3
		219.1	6.3	139.7	6.3	33.4	31.6	12.6	17.4	6.9	11.0
		219.1	5	139.7	5	34.7	28.2	10.0	21.9	7.8	13.1
$t_o < t_i$	Eq. (18)	219.1	10	114.3	10	42.4	45.8	20.0	11.0	4.8	7.2
		219.1	5	168.3	8	20.4	24.0	13.0	16.9	9.1	12.4
		219.1	5	139.7	6.3	34.7	28.7	11.3	19.4	7.6	12.2
		219.1	8	114.3	10	44.4	41.8	18.0	12.2	5.2	8.0

thicknesses t_{ring} and t_{gen} , calculated by Eqs. (15) to (18) and Eq. (21) respectively, proposed by the two-stage approach (Qian *et al.* 2015) for the ring model and the generator model in the pipe-in-pipe composite structures. All the sandwich composite pipes have the same length of $L = 2$ m as well as the same steel and cement composite strength, i.e., $\sigma_y = 400$ MPa and $f_c = 60$ MPa respectively.

Fig. 11 demonstrates the impact response for the fifteen pipe-in-pipe composite members under the four different impact velocities. For each composite pipe, the increase in the impact velocity indicates the rise of the external impact energy and thus leads to the increment of the impact force and the global displacement. Under the same impact velocity, the maximum impact force (P_{max}) decreases with the increase in the non-dimensional term $D_o / \sqrt{t_{gen} t_{ring}}$ (see Fig. 11(a)), implying that the structural capability for the composite pipe arises from the combined mechanism in the ring model and that in the generator model. The maximum global displacement (w_{max}) rises with the increase of the non-dimensional term D_o / t_{gen} (see Fig. 11(b)), indicating that the generator model contributes significantly to the global bending resistance of the composite pipe. Some composite pipes, i.e., outer pipe 219.1×10 with inner pipe 114.3×10 and outer pipe 219.1×8 with inner pipe 114.3×10, do not follow strictly the trend for the global displacement, as circled in Fig. 11(b). These two composite pipes exhibit larger global displacements than the expected values since they tend to dissipate a majority of the external impact energy by the global bending deformation and not by the local indentation. This indicates that the local indentation resistance for

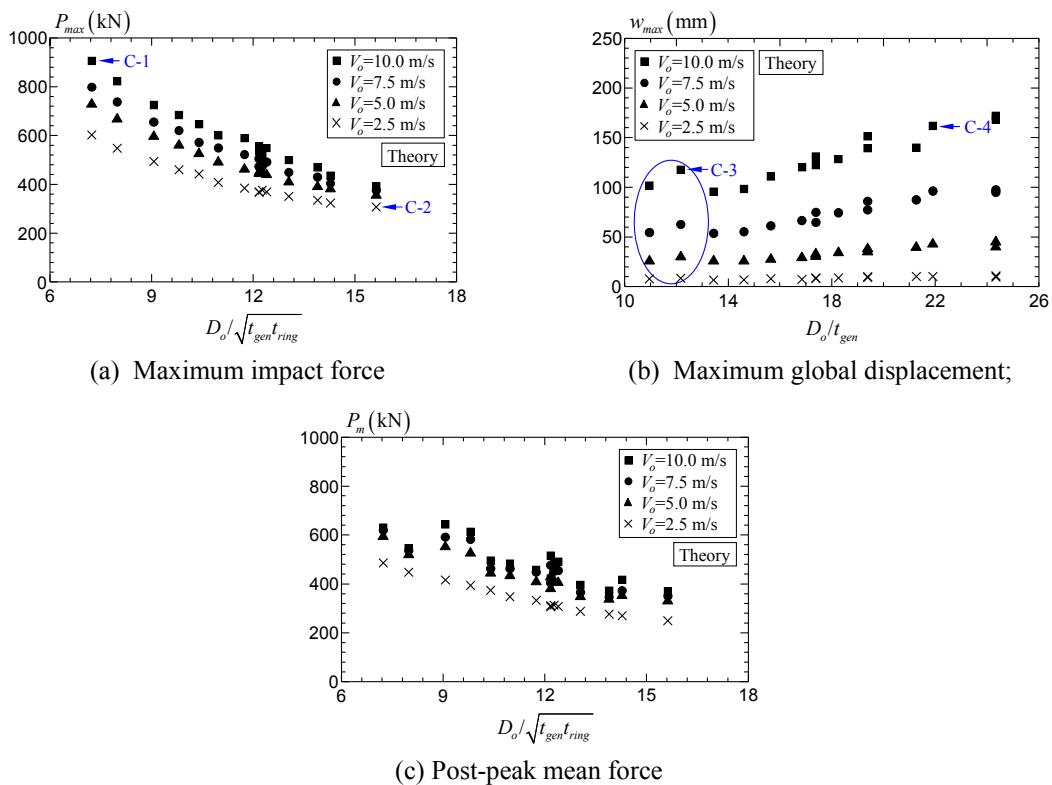


Fig. 11 Impact response (predicted by the theoretical model) for pipe-in-pipe composite members subjected to different impact velocities

Table 7 Details for the validation cases in the theoretical parametric study

Case	D_o (mm)	t_o (mm)	D_i (mm)	t_i (mm)	t_c (mm)	V_o (m/s)
C-1	219.1	10	114.3	10	42.4	10
C-2	219.1	5	168.3	4	20.4	2.5
C-3	219.1	8	114.3	10	44.4	10
C-4	219.1	6.3	168.3	4	19.1	10

Table 8 Comparison between the theoretical prediction and the FE results

Case	P_{\max} (kN)			w_{\max} (mm)			P_m (kN)		
	FE	Theory	Theory/FE	FE	Theory	Theory/FE	FE	Theory	Theory/FE
C-1	905.7	1024.0	0.88	101.7	108.3	0.94	630.0	606.8	1.04
C-2	307.3	291.6	1.05	9.4	11.3	0.83	249.0	255.9	0.97
C-3	821.8	858.5	0.96	117.8	123.5	0.95	545.8	529.0	1.03
C-4	435.6	460.1	0.95	139.8	141.0	1.00	415.9	415.6	1.00

Table 9 Inner pipe effect on the impact response for different pipe structures from FE analyses

Case	D_o (mm)	t_o (mm)	f_c (MPa)	D_i (mm)	t_i (mm)	P_{\max} (kN)	w_{\max} (mm)	P_m (kN)	δ_{\max} (mm)
CCFPIP-2-1	219.1	6.3	33.4	139.7	5.0	508.2	73.5	402.7	23.9
CCFPIP	219.1	6.3	33.4	139.7	6.3	537.7	70.6	406.9	21.9
CCFHP	219.1	6.3	33.4	-	-	253.5	97.5	235.3	84.2
HSP	219.1	6.3	-	-	-	250.8	288.1	86.7	149.8

the two composite pipes is quite high due to their thick-walled outer and inner steel pipes as well as the thick cement composite layer ($t_c > 40$ mm), as listed in Table 6. Fig. 11 highlights four typical theoretical prediction cases (see Table 7), including the cases which demonstrate the highest impact force (C-1), the lowest impact force (C-2), the overly high global displacement (C-3) and a relatively thin cement composite layer model (C-4). Table 8 and Fig. 12 compare the global impact response, predicted by the theoretical model and the FE procedure, for these four cases. The reasonable agreement between the theoretical prediction and the FE results confirms the accuracy of the theoretical predictions and the impact response observed in the parametric study (see Fig. 11) for a wide range of dimensions and under various impact velocities.

To investigate the effect of inner steel pipe on the impact performance of the pipe-in-pipe composite structure, this FE analysis examines the impact response for two pipe-in-pipe composite members with different inner pipe thicknesses, one hollow steel pipe as well as a fictitious cement composite filled hollow pipe by removing the inner steel pipe from the original pipe-in-pipe composite model. Table 9 presents the geometric properties for the four pipe models, in which "CCFPIP-2-1" and "CCFPIP" represent two cement composite filled pipe-in-pipe model with different inner pipe thicknesses ($t_i = 5$ mm and $t_i = 6.3$ mm), "CCFHP" refers to the cement composite filled hollow pipe model and "HSP" denotes the hollow steel pipe model with the same outer pipe thickness as the other three pipes. The four simulations utilize the same steel and cement composite strength, i.e., $\sigma_y = 400$ MPa and $f_c = 60$ MPa (if applicable), as well as the same

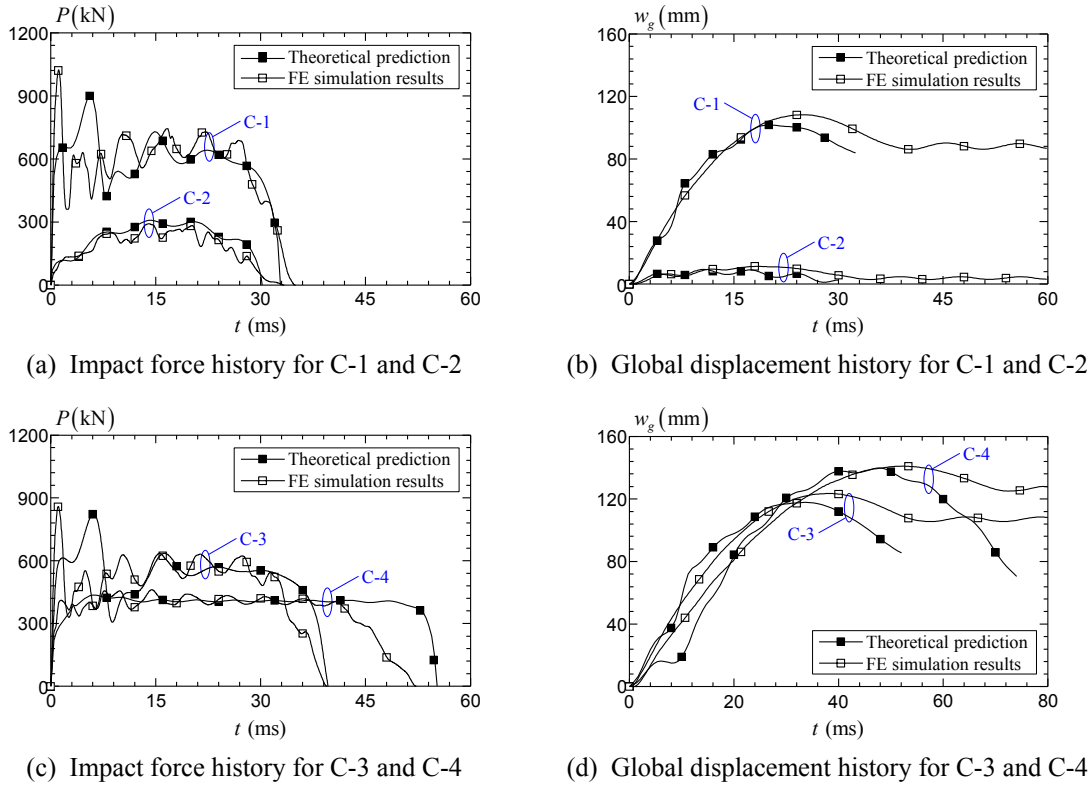


Fig. 12 Comparison of the impact response between the theoretical prediction and the FE simulation results for composite pipes

initial impact velocity ($V_o = 7.5$ m/s).

The impact responses for the two pipe-in-pipe composite models are quite close, with slight differences in the impact force, the global displacement, the local indentation and the stain values at the positions S-1 and S-2, as shown in Fig. 13. The increase in the inner pipe thickness leads to marginal increases in the maximum impact force (P_{max}) and the post-peak mean force (P_m) and slight decreases in the maximum global displacement (w_{max}) and the maximum local indentation (δ_{max}), as listed in Table 9.

In contrast, the impact response for CCFHP and the two sandwich composite pipes demonstrates significant differences, as illustrated in Fig. 13 and Table 9. Compared to CCFPIP-2-1, the impact force for CCFHP is apparently lower (Fig. 13(a)) while both the global and the local deformations (Figs. 13(b) and (c) respectively) for CCFHP are significantly larger due to the absence of the inner steel pipe. In the ULCC filled pipe-in-pipe composite structure, the inner steel pipe, together with the outer steel pipe, imposes a strong confinement effect to the infilled cement composite (the ULCC) and enhances significantly the composite action at large deformation levels. This steel-ULCC-steel composite action leads to improved impact resistance, small global and local deformations, for CCFPIP-2-1 under the transverse impact. Fig. 13(d) shows that the strains at S-1 and S-2 for CCFHP exceed that in CCFPIP-2-1, implying that the cement composite in CCFHP fails to provide effective constraint to the outer steel pipe, leading to the large deformation of the steel material at the quarter-span position. The hollow steel pipe, without the inner steel pipe

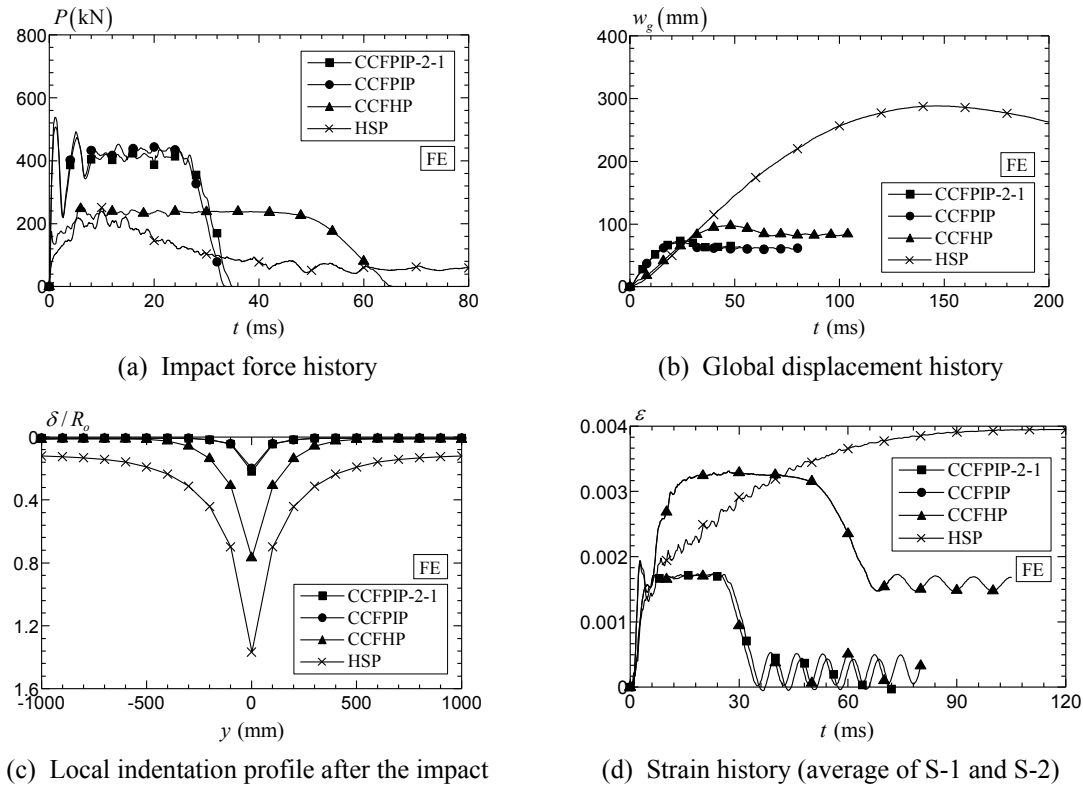


Fig. 13 Inner pipe effect on the impact response for different kinds of pipe structures

and the cement composite layer, demonstrates an extremely inferior impact performance under the transverse impact, as presented in Fig. 13 and Table 9.

3.3 Effect of material properties

In the previous study, Wang *et al.* (2014) employed S355 steel pipes (with a measured yield strength around 400 MPa) and ultra-lightweight cement composite (ULCC) (Chia *et al.* 2011) as the filler material for all the pipe-in-pipe composite specimens. The ULCC has a 28-day compressive strength over 60 MPa and an average density of 1460 kg/m³ (Wang *et al.* 2014), which is suitable for offshore structures. This section investigates the impact response of the pipe-in-pipe composite structures consisting of different steel and cement composite strengths, as well as different kinds of filler materials.

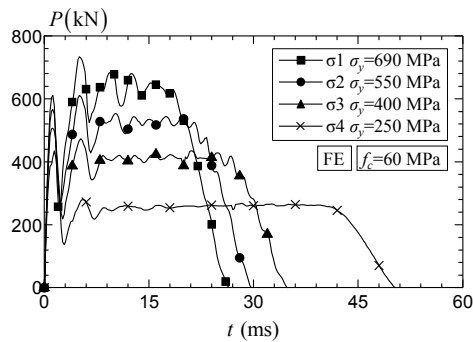
Table 10, Figs. 14 and 15 display the impact response for CCFPIP-2-1 consisting of commonly used structural steel pipes, with different yield strengths ranging from 250 MPa to 690 MPa. The FE procedure employs the experimental stress-strain curves from coupon tests in (Brockenbrough and Merritt 2006) and the theoretical model utilizes the corresponding strain-hardening exponents for steel pipes with different grades. In Table 10, “ σ_1 ”, “ σ_2 ”, “ σ_3 ” and “ σ_4 ” denote the composite pipes with the steel yield strength of 690 MPa, 550 MPa, 400 MPa and 250 MPa respectively. The four cases employ the same cement composite strength ($f_c = 60$ MPa) and the same initial impact velocity ($V_o = 7.5$ m/s). The impact responses predicted by the FE procedure and the theoretical

model demonstrate reasonable agreement, as listed in Table 10. Compared to the FE simulation results, the theoretical method overestimates the post-peak mean force (P_m) since the theoretical method ignores the cement composite failure during the impact, as discussed in Section 2.2.

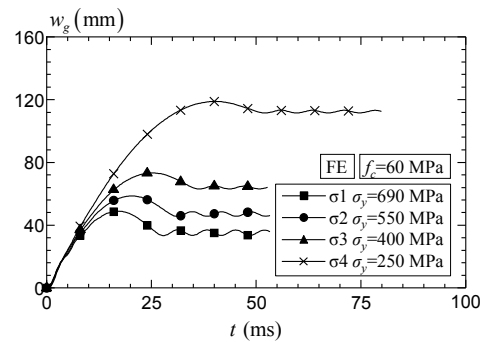
The increase in the yield strength of the steel pipes enhances both the global and the local resistance for the pipe-in-pipe composite structure, leading to the significant increase in the impact force, including the maximum impact force (P_{max}) and the post-peak mean force (P_m) as shown in Figs. 14(a) and 15(a), as well as the decrease of the global displacement (see Figs. 14(b) and 15(b)). Figs. 14(c) and 14(d) compare the maximum local indentation (δ_{max}) and the post-peak

Table 10 Impact response for CCFPIP-2-1 with different steel strength from FE analyses and theoretical predictions

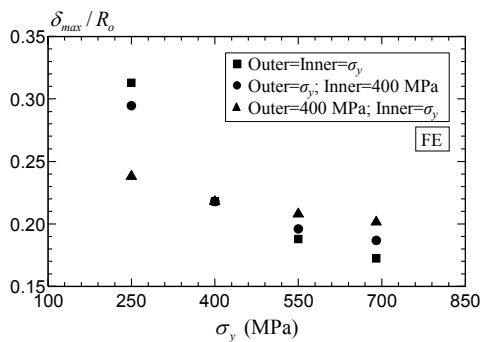
Case	σ_y (MPa)	f_c (MPa)	P_{max} (kN)			w_{max} (mm)			P_m (kN)			δ_{max} (mm)
			FE	Theory	Theory/FE	FE	Theory	Theory/FE	FE	Theory	Theory/FE	
σ_1	690	60	734.8	782.0	1.06	48.8	47.7	0.98	632.9	722.5	1.14	18.9
σ_2	550	60	611.5	637.1	1.04	58.6	59.5	1.02	521.0	580.5	1.11	20.6
σ_3	400	60	508.2	521.7	1.03	73.5	77.2	1.05	402.7	447.8	1.11	23.9
σ_4	250	60	426.7	371.6	0.87	118.8	127.2	1.07	253.4	288.5	1.14	34.3



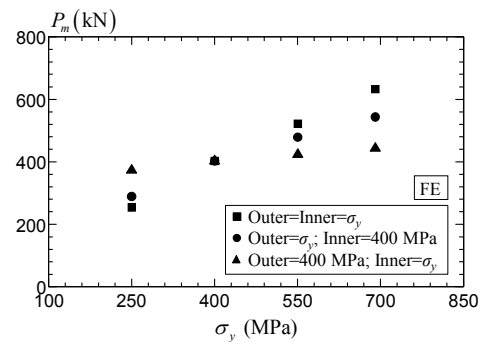
(a) Impact force history



(b) Global displacement history



(c) Maximum local indentation



(d) Post-peak mean force

Fig. 14 Comparison of the impact response (predicted by the FE procedure) for CCFPIP-2-1 with different steel strength

mean force (P_m), respectively, for three groups of pipe-in-pipe composite models with the same geometric properties as CCFPIP-2-1 but different strength combinations for the outer pipe and the inner pipe. In the first group, the outer pipe and the inner pipe consist of the same steel grade, with the yield strength ranging from 250 MPa to 690 MPa. In the second group, the yield strength of the outer pipe ranges from 250 MPa to 690 MPa while the inner pipe employs a fixed yield strength of 400 MPa. In the third group, the yield strength of the inner pipe covers 250 MPa to 690 MPa while the yield strength of the outer pipe utilizes a constant value of 400 MPa. All the pipe-in-pipe composite models in the three groups employ the same cement composite strength ($f_c = 60$ MPa) and experience the same initial impact velocity ($V_o = 7.5$ m/s). The increase in the outer pipe strength or the inner pipe strength both decreases the maximum local indentation (δ_{max}) and enhances the post-peak mean force (P_m). However, the increase in the outer pipe strength demonstrates a more significant effect on δ_{max} and P_m compared to the increase in the inner pipe strength (see Figs. 14(c) and (d)), indicating the dominant role of the outer pipe on the impact performance of the pipe-in-pipe composite structures.

Table 11 and Fig. 16 present the impact response for CCFPIP-2-1 containing the ultra-lightweight cement composite with the compressive strength ranging from 30 MPa to 90 MPa. In Table 11, “f1”, “f2” and “f3” denote the simulation cases with the cement composite compressive strength of 90 MPa, 60 MPa and 30 MPa respectively. The three cases utilize the same steel strength ($\sigma_y = 400$ MPa) and the same initial impact velocity ($V_o = 7.5$ m/s). The global impact

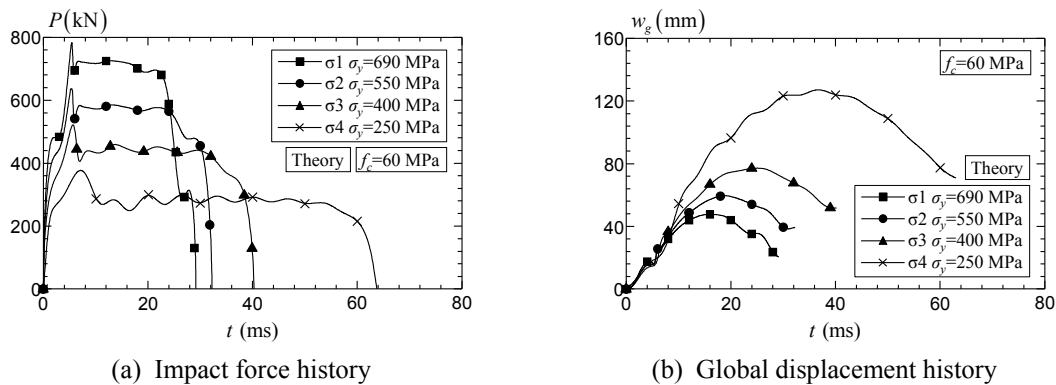


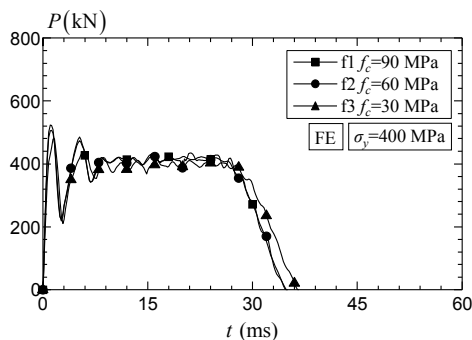
Fig. 15 Comparison of the impact response (predicted by the theoretical model) for CCFPIP-2-1 with different steel strength

Table 11 Impact response for CCFPIP-2-1 with different cement composite strength from FE analyses and theoretical predictions

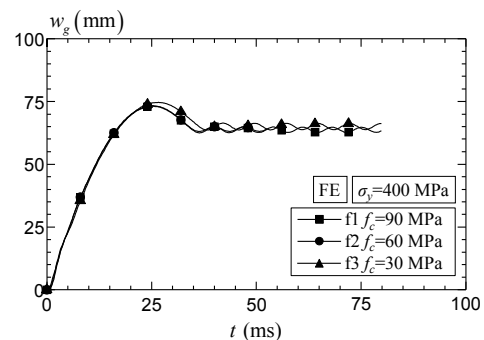
Case	σ_y (MPa)	f_c (MPa)	P_{max} (kN)			w_{max} (mm)			P_m (kN)			δ_{max} (mm)
			FE	Theory	Theory/FE	FE	Theory	Theory/FE	FE	Theory	Theory/FE	
f1	400	90	523.9	523.2	1.00	73.1	76.9	1.05	406.5	448.1	1.10	23.7
f2	400	60	508.2	521.7	1.03	73.5	77.2	1.05	402.7	447.8	1.11	23.9
f3	400	30	479.3	438.0	0.91	74.6	81.1	1.09	378.1	405.9	1.07	28.0
f1	400	90	523.9	523.2	1.00	73.1	76.9	1.05	406.5	448.1	1.10	23.7

responses predicted by the FE procedure and the theoretical model demonstrate reasonable agreement, as listed in Table 11. Compared to the FE results, the theoretical method overestimates the maximum global displacement (w_{max}) as the theoretical method neglects energy losses and over-predicts the post-peak mean force (P_m) due to the ignorance of the cement composite failure during the impact, as discussed in Section 2.2.

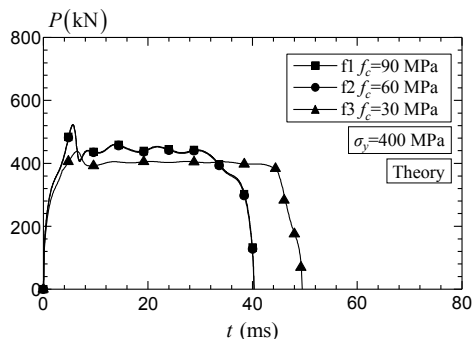
Fig. 16 presents the effect of compressive strength on the impact response of the pipe-in-pipe composite specimens calculated from the FE procedure (Figs. 16(a) and (b)) and from the theoretical model (Figs. 16(c) and (d)). Compared to the steel material, the increase in the compressive strength of the cement composite, especially from 60 MPa to 90 MPa, presents small influences on the impact force response (see Figs. 16(a) and (c)) as well as a slight enhancement on the global displacement for the pipe-in-pipe composite structures (see Figs. 16(b) and (d)). This indicates the limited contribution from the strength increment of the cement composite to the impact response for the pipe-in-pipe composite structure. When the compressive strength of the cement composite decreases from 60 MPa to 30 MPa, the global impact response (predicted by the theoretical approach) presents some differences (see Figs. 16(c) and (d)). In the theoretical approach, the P - δ response for the composite pipe has transitioned from the first composite stage (Eq. (22)) to the second separation stage (Eq. (23)) due to the decrease in the cement composite strength (from 60 MPa to 30 MPa) at a small indentation level. This transition indicates the decrease of the composite action for the sandwich pipe, leading to the reduction in the impact force (for both the maximum impact force P_{max} and the post-peak mean force P_m) and the increase in the



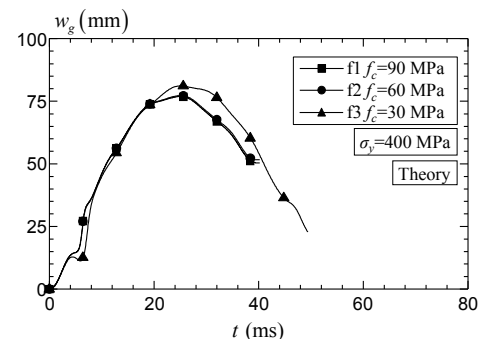
(a) Impact force history predicted by FE



(b) Global displacement history predicted by FE



(c) Impact force history by theoretical model



(d) Global displacement history by theoretical model

Fig. 16 Comparison of the impact response for CCFPIP-2-1 with different cement composite strength

global displacement. In the FE analyses (shown in Table 11), the maximum local indentation (δ_{max}) decreases significantly by about 15% when the cement composite strength improves from 30 MPa to 60 MPa while drops marginally (within 1%) when the cement composite strength increases from 60 MPa to 90 MPa. The local indentation does not decrease significantly when the cement composite strength reaches some level, i.e., 60 MPa in the current FE simulations.

Besides the strength of the filler material (the ULCC), this study also investigates the effect of different kinds of filler materials on the impact response for the pipe-in-pipe composite structures by the FE method. Table 12 and Fig. 17 demonstrate the impact response of the pipe-in-pipe composite structure filled with the ultra lightweight cement composite (the ULCC), the normal weight concrete and one kind of high strength grout (NaX™ Q110) developed by Nautic Group, respectively. In Table 12, “ULCC”, “Normal weight concrete” and “NaX™ Q110” refer to the FE simulations for the ULCC-filled, the normal weight concrete filled and the high strength grout filled pipe-in-pipe composite structures. The FE simulation employs the same material model (type MAT_72R3 in LS-DYNA) but different parameters based on the material tests (e.g., compressive strength f_c , density ρ_c and elastic modulus E_c as listed in Table 12) to describe the behavior of the three filler materials. The FE analyses utilize the pipe-in-pipe composite model with the same geometric properties as CCFPIP-2-1 and the same steel strength ($\sigma_y = 400$ MPa) as well as the same initial impact velocity ($V_o = 7.5$ m/s).

The impact response between the pipe-in-pipe composite structures filled with the three kinds of materials are quite similar, as illustrated in Fig. 17 and Table 12. At the initial phase of the

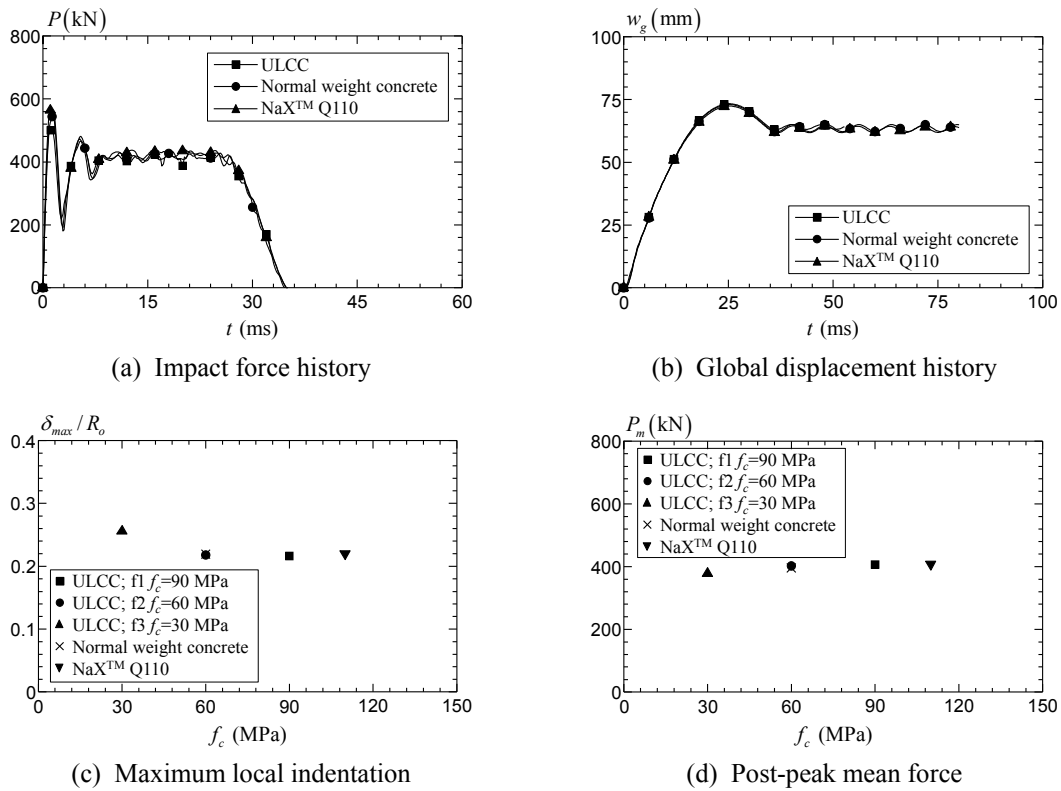


Fig. 17 Comparison of the impact response for CCFPIP-2-1 with different kinds of filler materials

Table 12 Impact response for CCFPIP-2-1 with different filler materials from FE analyses

Case	f_c (MPa)	ρ_c (kg/m ³)	E_c (GPa)	m_p (kg)	P_{max} (kN)	w_{max} (mm)
ULCC	60	1470	16.9	152.0	508.2	73.5
Normal weight concrete	60	2400	37.0	186.5	558.2	73.0
NaX TM Q110	110	2320	37.0	183.6	569.2	72.4

impact, the impact force accelerates the composite pipe from the zero velocity to a speed approaching that of the drop weight. Under the same impact velocity, the normal weight concrete filled pipe-in-pipe model ($m_p = 186.5$ kg) demonstrates a slightly higher peak force (P_{max}) than that for the ULCC filled pipe-in-pipe model ($m_p = 152.0$ kg) due to its heavier weight from the heavier filler material. The high strength grout filled pipe-in-pipe composite model presents the highest peak force (P_{max}) among the three pipes for its heavy weight ($m_p = 183.6$ kg) and the high strength fillers ($f_c = 110$ MPa), as shown in Table 12. However, the increase in the filler material strength exhibits limited effect on the peak force (P_{max}) for the pipe-in-pipe model filled with NaXTM Q110 compared to the pipe-in-pipe model filled with normal weight concrete (see Table 12). Figs. 17(c) and (d) display the maximum local indentation (δ_{max}) and the post-peak mean force (P_m), respectively, for the five pipe-in-pipe composite models filled with ULCC with three different compressive strengths, the normal weight concrete and the high strength grout (NaXTM Q110). The maximum local indentation (δ_{max}) for the four sandwich composite pipes with $f_c \geq 60$ MPa are quite close but increases apparently when the compressive strength of the filler material decreases from 60 MPa to 30 MPa, as illustrated in Fig. 17(c). The pipe-in-pipe composite models filled with five different materials demonstrate the similar post-peak mean force (P_m), as shown in Fig. 17(d). These again prove the slight influence of the filler material on the impact response of the pipe-in-pipe composite structures especially when the filler material strength reaches some level, i.e. 60 MPa in the current parametric study.

4. Conclusions

This paper presents a parametric study using both a validated FE procedure and a validated theoretical approach on the transverse impact response for the ULCC-filled pipe-in-pipe composite structures. The FE procedure predicts not only the global impact response but also the detailed local impact response for the pipe-in-pipe composite structures. On the other hand, the theoretical approach provides fast and reasonable predictions on the global impact response for the composite pipe structures covering a wide scope of geometric properties. The parametric study investigates the effect of the impact loading conditions (including the impact velocity and the indenter shape), the geometric properties (including the pipe length and the dimensions of the three material layers) as well as the material properties (including the material properties of the steel pipe and the filler materials) on the impact response for the pipe-in-pipe composite structure. This study supports the following observations and conclusions:

- (1) The maximum impact force (P_{max}) increases with the increase of the impact velocity (V_o), the yield strength of the steel pipe (σ_y) and the mass of the composite pipe (m_p). The contact area between the impact indenter and the pipe specimen influences the force transfer during the initial strike and causes the maximum impact force (P_{max}) to increase

with the increasing contact area.

- (2) The post-peak mean force (P_m) provides a good reference to the real structural capacity of the pipe-in-pipe composite member under external impacts. The post-peak mean force P_m relies significantly on the yield strength of the steel pipe (σ_y) and the flexural stiffness of the pipe [corresponding to different pipe lengths (L) in this study]. The increases in the yield strength of the steel pipe (σ_y) and the flexural stiffness of the pipe [i.e., the decrease in the pipe length (L)] enhance significantly the post-peak mean force P_m .
- (3) Both the global displacement (w_g) and the local indentation (δ) intensify with the increase of the initial impact velocity (V_o) and the decrease of the steel pipe strength (σ_y). The global displacement (w_g) increases with the increase of the pipe length (L) while the local indentation (δ) decreases with the increase of the pipe length (L). In addition, the local indentation (δ) escalates with the decrease of the contact area between the indenter and the composite pipe.
- (4) The theoretical parametric study covering a wide scope of geometric properties ($D_o/t_o \in [21.9, 43.8]$, $D_i/t_i \in [11.4, 42.1]$ and $t_c \in [15.4 \text{ mm}, 44.4 \text{ mm}]$) for the composite pipes under various impact velocities (V_o) presents the general trends between the global impact response and the proposed equivalent thicknesses t_{ring} and t_{gen} . When the P - δ response for the ULCC-filled pipe-in-pipe composite structures remains within the first composite stage, the maximum impact force (P_{max}) decreases with the increase in the non-dimensional term $D_o / \sqrt{t_{gen} t_{ring}}$ while the maximum global displacement (w_{max}) rises with the increase of the non-dimensional term D_o / t_{gen} . The FE simulations confirm the accuracy of the theoretical parametric study and the trends.
- (5) In the pipe-in-pipe composite structure, the inner steel pipe, together with the outer steel pipe, imposes a strong confinement to the infilled cement composite (the ULCC) and enhances significantly the composite action, leading to improved impact resistance, small global and local deformations. The strength and the type of the filler materials demonstrate negligible influences on the impact response of the pipe-in-pipe composite structures.

Acknowledgments

The authors would like to acknowledge the financial support from the Academic Research Fund Tier 1 (Grant No. R-302-501-020-112) and Agency for Science Technology and Research (SERC Grant No.: 1123004035) provided by Singapore and the research scholarship offered to the first author by the China Scholarship Council.

References

- ABAQUS (2010), ABAQUS/Standard User's Manual; Hibbitt Karlsson and So-rensens Inc., Rising Sun Mills, RI, USA.
- An, C., Castello, X., Duan, M., Filho, R.D.T. and Estefen, S.F. (2012), "Ultimate strength behavior of sandwich pipes filled with steel fiber reinforced concrete", *Ocean Eng.*, **55**, 125-135.
- Arabzadeh, H. and Zeinoddini, M. (2011), "Dynamic response of pressurized submarine pipelines subjected to transverse impact loads", *Procedia Eng.*, **14**, 648-655.
- Arjomandi, K. and Taheri, F. (2011), "Stability and post buckling response of sandwich pipes under hydrostatic external pressure", *Int. J. Press Vessels Pip.*, **88**(4), 138-148.
- Brockenbrough, R.L. and Merritt, F.S. (2006), *Structural Steel Designer's Handbook: AISC, AASHTO, AISI*,

- ASTM and ASCE-07 Design Standards*; McGraw, Inc., New York, NY, USA.
- Brooker, D.C. (2005), "Experimental puncture loads for external interference of pipelines by excavator equipment", *Int. J. Press Vessels Pip.*, **82**(11), 825-832.
- Chia, K.S., Zhang, M.H. and Liew, J.Y.R. (2011), "High-strength ultra lightweight cement composite material properties", *Proceedings of 9th International Symposium on High Performance Concrete-Design, Verification & Utilization*, Primary Section A8-paper 2.
- Comité Euro-International du Béton (CEB) (1993), CEB-FIP Model Code 1990; Redwood Books, Trowbridge, Wiltshire, UK.
- Crupi, V., Epasto, G. and Guglielmino, E. (2011), "Low-velocity impact strength of sandwich materials", *J. Sandw. Struct. Mater.*, **13**(4), 409-426.
- DNV-RP-F107 (2010), Risk Assessment of Pipeline Protection; Recommended practice, Det Norske Veritas (DNV).
- DNV-RP-F111 (2010), Interference between Trawl Gear and Pipelines; Recommended practice, Det Norske Veritas (DNV).
- Ding, X., Fan, Y., Kong, G. and Zheng, C. (2014), "Wave propagation in a concrete filled steel tubular column due to transient impact loading", *Steel Compos. Struct., Int. J.*, **17**(6), 891-906.
- Famiyesin, O.O.R., Oliver, K.D. and Rodger, A.A. (2002), "Semi-empirical equations for pipeline design by the finite element method", *Comput. Struct.*, **80**(16-17), 1369-1382.
- Goldsmith, W. (1960), *Impact, the Theory and Physical Behavior of Colliding Solids*, Edward Arnold Publishers, London, UK.
- Hallquist, J.O. (2006), LS-DYNA keyword user manual-nonlinear dynamic analysis of structures; Livermore Software technology Corporation, Livermore, CA, USA.
- Han, L.H., Huang, H., Tao, Z. and Zhao, X.L. (2006), "Concrete-filled double skin steel tubular (CFDST) beam-columns subjected to cyclic bending", *Eng. Struct.*, **28**(12), 1698-1714.
- Jankowiak, A.R., Kpenyigba, K.M. and Pesci, R. (2014), "Ballistic behavior of steel sheet subjected to impact and perforation", *Steel Compos. Struct., Int. J.*, **16**(6), 595-609.
- Jones, N. and Birch, R.S. (2010), "Low-velocity impact of pressurized pipelines", *Int. J. Impact Eng.*, **37**(2), 207-219.
- Jones, N., Birch, S.E., Birch, R.S., Zhu, L. and Brown, M. (1992), "An experimental study on the lateral impact of fully clamped mild steel pipes", *Proc. Instn. Mech. Eng. E. J. Process. Mech. Eng.*, **206**, 111-127.
- Kantar, E. and Anil, O. (2012), "Low velocity impact behavior of concrete beam strengthened with CFRP strip", *Steel Compos. Struct., Int. J.*, **12**(3), 207-230.
- Kharazan, M., Sadr, M.H. and Kiani, M. (2014), "Delamination growth analysis in composite laminates subjected to low velocity impact", *Steel Compos. Struct., Int. J.*, **17**(4), 387-403.
- Lee, E.H. (1940), "The impact of a mass striking a beam", *J. Appl. Mech.*, **7**, A129-38.
- Li, W., Han, L.H. and Zhao, X.L. (2012), "Axial strength of concrete-filled double skin steel tubular (CFDST) columns with preload on steel tubes", *Thin-Wall. Struct.*, **56**, 9-20.
- Malekzadeh, F.K. (2014), "Higher order impact analysis of sandwich panels with functionally graded flexible cores", *Steel Compos. Struct., Int. J.*, **16**(4), 389-415.
- Malvar, L.J. and Ross, C.A. (1998), "Review of strain rate effects for concrete in tension", *ACI Mat. J.*, **95**(6), 735-739.
- Malvar, L.J., Crawford, J.E., Wesevich, J.W. and Simons, D. (1997), "A plasticity concrete material model for DYNA3D", *Int. J. Impact Eng.*, **19**(9-10), 847-873.
- Mamalis, A.G., Manolakos, D.E., Ioannidis, M.B. and Kostazos, P.K. (2010), "Bending of cylindrical steel tubes: numerical modeling", *Int. J. Crashworthiness*, **11**(1), 37-47.
- Ng, C.S. and Shen, W.Q. (2006), "Effect of lateral impact loads on failure of pressurized pipelines supported by foundation", *Proc. Instn. Mech. Eng. E. J. Process Mech. Eng.*, **220**, 193-206.
- Qian, X., Wang, Y., Liew, J.Y.R. and Zhang, M.H. (2015), "A load indentation formulation for cement filled pipe-in-pipe composite structures", *Eng. Struct.*, **92**, 84-100.
- Richardson, M.O.W. and Wishear, M.J. (1996), "Review of low-velocity impact properties of composite

- materials”, *Compos. A Appl. Sci. Manuf.*, **27A**(12), 1123-1131.
- Shen, W.Q. and Shu, D.W. (2002), “A theoretical analysis on the failure of unpressurized and pressurized pipelines”, *Proc. Instn. Mech. Eng. E. J. Process Mech. Eng.*, **216**(0), 151-164.
- Sohel, K.M.A. (2008), “Impact performance of steel-concrete-steel sandwich structures”, Ph.D. Dissertation; National University of Singapore, Singapore.
- Thomas, S.G., Reid, S.R. and Johnson, W. (1976), “Large deformations of thin-walled circular tubes under transverse loading-I An experimental survey of the bending of simply supported tubes under a central load”, *Int. J. Mech. Sci.*, **18**(6), 325-333.
- Uenaka, K. and Kitoh, H. (2011), “Mechanical behavior of concrete filled double skin tubular circular deep beams”, *Thin-Wall. Struct.*, **49**(2), 256-263.
- Uenaka, K., Kitoh, H. and Sonoda, K. (2010), “Concrete filled double skin circular stub columns under compression”, *Thin-Wall. Struct.*, **48**(1), 19-24.
- Wang, Y. (2015), “Impact performance of cement composite filled pipe in pipe structures”, Ph.D. Dissertation; National University of Singapore, Singapore.
- Wang, Y., Qian, X., Liew, J.Y.R. and Zhang, M.H. (2014), “Experimental behavior of cement filled pipe-in-pipe composite structures under transverse impact”, *Int. J. Impact Eng.*, **72**, 1-16.
- Wang, Y., Qian, X., Liew, J.Y.R. and Zhang, M.H. (2015), “Impact of cement composite filled steel tubes: an experimental, numerical and theoretical treatise”, *Thin-Wall. Struct.*, **87**, 76-88.
- Wen, H.M. (1997), “Large plastic deformation of spherical shells under impact by blunt-ended missiles”, *Int. J. Press. Vessels Pip.*, **73**(2), 147-152.
- Wen, H.M. and Reid, S.R. (1998), “Deformation and perforation of cylindrical shells struck normally by blunt projectiles”, *Int. J. Press. Vessels Pip.*, **75**(3), 213-219.
- Wierzbicki, T. and Suh, M.S. (1988), “Indentation of tubes under combined loading”, *Int. J. Mech. Sci.*, **30**(3-4), 229-248.
- Xie, Z., Yan, Q. and Li, X. (2014), “Investigation on low velocity impact on a foam core composite sandwich panel”, *Steel Compos. Struct., Int. J.*, **17**(2), 159-172.
- Yang, J.L., Lu, G.Y., Yu, T.X. and Reid, S.R. (2009), “Experimental study and numerical simulation of pipe-on-pipe impact”, *Int. J. Impact Eng.*, **36**(10-11), 1259-1268.
- Yang, Y.F., Han, L.H. and Sun, B.H. (2012), “Experimental behavior of partially loaded concrete filled double-skin steel tube (CFDST) sections”, *J. Constr. Steel Res.*, **71**, 63-73.
- Zhang, Y.F., Zhao, J.H. and Cai, C.S. (2012), “Seismic behavior of ring beam joints between concrete-filled twin steel tubes columns and reinforced concrete beams”, *Eng. Struct.*, **39**, 1-10.
- Zhao, X.L. and Han, L.H. (2006), “Double skin composite construction”, *Prog. Struct. Eng. Mater.*, **8**(3), 93-102.
- Zhao, X.L., Tong, L.W. and Wang, X.Y. (2010), “CFDST stub columns subjected to large deformation axial loading”, *Eng. Struct.*, **32**(3), 692-703.
- Zeinoddini, M., Parke, G.A.R. and Harding, J.E. (2002), “Axially pre-loaded steel tubes subjected to lateral impacts: an experimental study”, *Int. J. Impact Eng.*, **27**(6), 669-690.
- Zeinoddini, M., Harding, J.E. and Parke, G.A.R. (2008a), “Axially pre-loaded steel tubes subjected to lateral impacts: a numerical simulation”, *Int. J. Impact Eng.*, **35**(11), 1267-1279.
- Zeinoddini, M., Parke, G.A.R. and Harding, J.E. (2008b), “Interface forces in laterally impacted steel tubes”, *Proc. Soc. Exp. Mech.*, **48**(3), 265-280.
- Zeinoddini, M., Arabzadeh, H., Ezzati, M. and Parke, G.A.R. (2013), “Response of submarine pipelines to impacts from dropped objects: bed flexibility effects”, *Int. J. Impact Eng.*, **62**, 129-141.